Microfluidic Fuel Cells – Modeling and Simulation

Boming Zhu

A Thesis

In the Department

of

Mechanical and Industrial Engineering

Presented in Partial Fulfillment of the Requirements

For the Degree of Master of Applied Science

(Mechanical Engineering) at

Concordia University

Montréal, Québec, Canada

December 2010

CONCORDIA UNIVERSITY

SCHOOL OF GRADUATE STUDIES

This is to certify that the Thesis prepared,

By: **Boming ZHU**

Entitled: **"Microfluidic Fuel Cell – Modeling and Simulation"**

and submitted in partial fulfillment of the requirements for the Degree of

Master of Applied Science (Mechanical Engineering)

complies with the regulations of this University and meets the accepted standards with respect to originality and quality.

Signed by the Final Examining Committee:

Dr. A.K.W. Ahmed	Chair
Dr. P. Wood-Adams	Examiner
Dr. S. Omanovic Chemical Engineering, McGill University	Examiner External
Dr. L. Kadem	Co-Supervisor
Dr. R. Wuthrich	Co-Supervisor

Approved by:

Dr. A.K.W. Ahmed, MASc Program Director
Department of Mechanical and Industrial Engineering

Dean Robin Drew
Faculty of Engineering & Computer Science

Date:

ABSTRACT

Microfluidic Fuel Cells – Modeling and Simulation

Boming Zhu

Microfluidic fuel cells are a novel fuel cell design that uses laminar flow to operate without a solid barrier separating fuel and oxidant. This makes it possible to have an efficient fuel cell that can provide cheap and effective power for small electronic devices. Microfluidic fuel cells show great promise as an alternative energy source for lowering the cost and scaling down the size of fuel cells. The focus of this dissertation is to build a numerical microfluidic fuel cell model in COMSOL Multiphysics® to investigate transport phenomenon and electochemical reactions.

In order to develop the numerical model of the microfluidic fuel cell, a theoretical study on mass transfer, hydrodynamics and electrochemistry has been presented. Afterward, a benchmark model for a cottrell experiment is presented to verify our theoretical environment for modeling in COMSOL Multiphysics®. Then, a study of microfluidic fuel cell modeling with 2-Dimensional and 3-Dimensional geometry is presented.

At the end, a detailed analysis on the modeling results has been presented. It shows that Y-shaped microchannel with 45° convergence angle design has the best cell performance rather than other angles. In addition, modifying the volumetric flow rate, reactants concentration, and catalyst layer can also improve the cell performance.

ACKNOWLEDGEMENTS

There are many people have helped me in my master study, without any of them, this original thesis would never have been completed. I gladly would like to express sincere thanks to my supervisors, Dr. Rolf Wuthrich and Dr. Lyes Kadem, who have provided dedicated guidance, instruction and support through my studies. As mentors, they provided me excellent support and guidance throughout all aspects of my research. It has been a true privilege to work with them and share their combined expertise and experience essential to this dissertation.

I would also like to thank Prof. Philippe Mandin and Dr. Muriel Carin for their generosity of time through many discussions that made significant contribution to this work when I was working in France.

I am also grateful to my friends and colleagues in the ECD laboratory for their many contributions to this work, most notably Anis Allagui, Alexandre Teixeira, Andrew Morrison and Jayan Ozhikandathil.

Finally, without the understanding and the supporting of my beloved family back in China, I would not have been able to focous on my stuies. Many thanks are due to my parents, Mr. Zhu Chuan Zhong and Mrs. Yang Xia, whose infinite generosity and profound admiration for research and science offered a great deal of support while overcoming most of the difficulties encountered during this work.

Boming Zhu

Dedicated with much love, affection and gratitude to my father and mother.

TABLE OF CONTENTS

LIST OF FIGURES

LIST OF TABLES

Chapter 1

INTRODUCTION

It is a more and more accepted sense now that fuel cells are one of the most fascinating and interesting aspects of today's technology. The interest in fuel cells has been intensified during the past decade due to the fact that the use of fossil fuels for generating power has resulted in several negative consequences, including severe pollutions, exhaustive exploitation of the global resources, and imbalance in political power caused by uneven distribution of natural resources. Such problems underline the need for a new power source-fuel cell, which is energy efficient, environmental friendly and renewable. Fuel cells are now closer to commercialization than ever, and they have the potential in helping to fulfill the world's demand for power and at the same time reach the requirement and the expectation on environmental protection. Despite all the advantages enumerated above, this field is still under development. Under the influence of booming MEMS technology, the fabrication of microscale devices has experienced a considerable growth. As a result, the demands for energy resources used in portable devices are under continual pressure to decrease both consumed power and weight. Both

demands can be satisfied well by miniaturized power resource, such as microfluidic fuel cell.

1.1 Microfluidic Fuel Cell

A fuel cell is an electrochemical conversion device. It produces electricity with fuel (on the anode side) and an oxidant (on the cathode side), in the presence of an electrolyte. The reactants flow into the cell, and the reaction products flow out of it, while the electrolyte remains within it. Fuel cells can operate virtually continuously as long as the necessary flows are maintained. Since it is effective and environmentally friendly, it is getting an increasingly wide popularity. Presently, fuel cells have been used in automobiles and space shuttle, even for cell phones and lap tops.

Proton exchange membrane(PEM) fuel cell, also known as polymer electrolyte membrane fuel cell (PEMFC),are suitable for various applications such as transport applications, and both stationary and portable fuel cell applications.

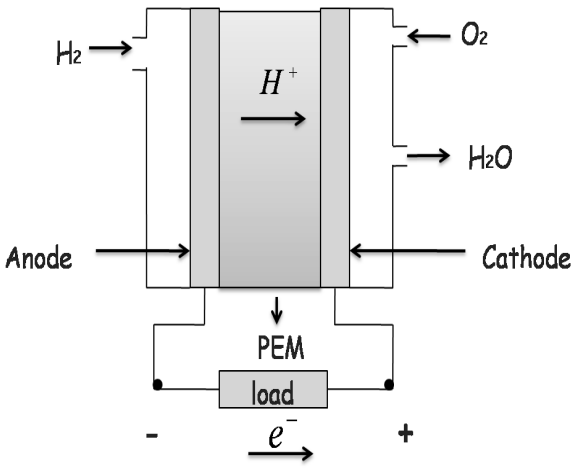

Figure 1.1: PEMFC theoretical design

The PEMFC uses gaseous hydrogen as fuel and oxygen from the ambient air as oxidant. As shown in Figure 1.1, the membrane is sandwiched between the catalyst

layers, gas-diffusion electrodes, and bipolar plates for the anode and cathode. From the two bipolar plates(containing fuel-left and oxidant-right flow channels), the reactants diffuse through the gas-diffusion electrodes and react at the catalyst layers, the protons released at the anode reaction travel through the ion conducting membrane, and the electrons released follow an external path. The redox reactions at the anode and cathode drive the operation of the fuel cell by producing an electric potential and a current through an applied load.

Nevertheless, the PEMFC has problems associated with its operation. High temperatures can improve the efficiency of fuel cells due to fast kinetics, but on the other hand tend to dry out the PEM, reducing the effectiveness of proton conduction. Thus water management becomes crucial since the PEM has to be kept hydrated at all times in order to facilitate the transport of protons. Another significant problem for PEMFC is fuel crossover through the membrane, which results in a mixed potential at the cathode and thereby lowers the cell performance. Despite extensive efforts, these problems still remain major obstacles preventing PEMFC from wide-scale portable applications (*4*).

Based on those problems mentioned above, a new type of fuel cell comes out to overcome these issues – the Microfluidic Fuel Cell defined as a fuel cell with fluid transport, reaction sites and electrode structures all confined to a microfluidic channel. This type of fuel cell operates without a physical barrier, such as a membrane which is a costly component in the fuel cell devices, to separate the anode and the cathode, and can use both metallic and biological catalysts. For a most typical architecture of micorfluidic fuel cell, it operates in a co-laminar flow which is able to delay convective mixing of fuel and oxidant. The laminar flow regime is characterized by high momentum diffusion and low momentum convection which can be presented by Reynold's number, usually at a low Reynolds' number, the two aqueous streams, one containing the fuel and the other containing the oxidant, will flow in

parallel layers down a single microfluidic channel, with no disruption between the layers, as shown in Figure 1.2. This design makes it possible to avoid many of the issues associated with polymer electrolyte membrane-based fuel cells, for example, humidification, membrane degradation, and fuel crossover. In the microchannel, the anolyte and catholyte contain supporting electrolyte that facilitates ionic transport within the streams, thereby eliminating the need for a separate electrolyte. In the channel, where the stream mixing taking place, only has proton exchange by transverse diffusion, which is restricted to an interfacial width at the center. There are various factors affecting the width of mixture, such as flow rate and channel dimensions. Meanwhile, it is also necessary to keep the electrodes away from the co-laminar inter-diffusion zone in order to avoid fuel crossover. Since the electrochemical reactions occurring in fuel cells are surface based, increasing the surface to volume ratio accompanying miniaturization improves the performance of fuel cell. In addition, microfluidic cells also fulfill the needs of portable devices for micro scale power sources, such as cell phones and laptop computers. Most appreciably, the microfluidic fuel cells can be manufactured in an expensive way, by Spark Assisted Chemical Engraving (SACE) machining in Dr. Wuthrich's lab. SACE is a novel method for 3D microstructuring of glass or other nonconductive materials with high aspect ratio and smooth surface quality (*5*), which can significantly decrease the cost of microfludic fuel cells manufacture. Besides, microfluidic fuel cells are usually operated at room temperature which can avoid the auxiliary humidification, water management, and cooling systems. However, before all the advantages of micorfluidic fuel cells mentioned above can be possibly capitalized, relative work should be done about the energy density and fuel utilization. (*6*).

The majority of microchannel devices employed a Y-(*4*) or T-shaped(*7*) microfluidic channel design featuring two aqueous co-laminar streams with fuel and oxidant

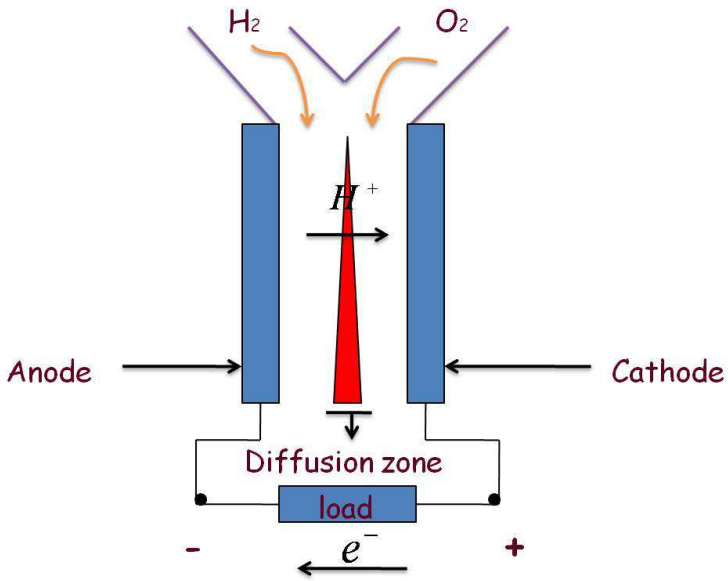

Figure 1.2: Microfluidic Fuel Cells theoretical design

dissolving in a supporting electrolyte and electrodes on the opposite channel walls parallel to the inter-diffusion zone.

The two physicochemical phenomena that govern the chemical conversion and the energy and mass transport phenomena in these laminar flow-based fuel cells occurring at the same time are examined. They are(i) depletion of reactants at the electrode walls and (ii) diffusion across the mutual liquid-liquid interface. An external reference electrode has also been introduced, enabling separate and simultaneous assessment of the individual performance of the anode and cathode in a single experiment. This method for direct evaluation of the anode and cathode performance through the use of an external reference electrode provides an excellent tool for system analysis.

A limiting factor in the operation of the laminar flow-based microfluidic fuel cell is the low solubility of oxygen in solution which causes significant mass transfer limitations during higher current operation. In addition, depletion boundary layers form as a result of fuel and oxidant reacting on the anode and cathode respectively,

causing mass transfer limitations as well. The choice of catalyst, fuel and oxidant is therefore crucial for performance optimization.

1.2 Aims and Motivations

In this thesis, the fundamentals behind microfluidic fuel cell technology will be described first. The following part will present the development of microfluidic fuel cells to date. Series consideration will be given to choice of reactants, electrochemical reactions, transport characteristics and, particularly here, cell architectures. Microfluidic fuel cell architecture is an area that has seen particularly rapid development, as discussed by Bazylak et al. (*7*). In oder to solve those problems mentioned previously, on the one hand, a mathematical model has been built to study the single and linked simultaneous reactions occurring at the cathode electrode of the microfluidic fuel cell. The reason for focusing only on the cathode-side reactions originates from a report (*4*) which mention that the entire current density cannot increase significantly with the fuel concentration but can be limited obviously by the low oxidant concentration. The experiments(*4*) showed that the cell's performance was cathode limited. Accordingly, this thesis has been concentrated on developing three-dimensional half cell models for studying the cases of single reaction and linked simultaneous reactions occurring at the cathode.

It begins with the governing equations for the steady incompressible parallel flows. Mass transport equations and Navier-Stokes equation have been solved as well; On the other hand, by using COMSOL® which is a multiphysic software able to combine several phenomena based on polarization curves, and a numerical model has been developed to determine the effect of the channel geometry on cell performance. The Butler-Volmer model is used to determine the reaction rates at the electrodes. Two Conductive Media DC modules representing electronic transport

in the external circle and ionic transport in the internal circle respectively are used to model the electric fields within the fuel cell. The concentration distributions of the reactant species and velocity distributions of the flow are obtained by using the Incompressible Navier-Stokes and Convection and Diffusion modules. Solving these equations together predicts the current density for the given cell voltage values. The results demonstrate the cell voltage losses due to activation, ohmic and concentration overpotentials. By changing the model geometry to minimize these overpotentials, this computational tool plays a critical role in the design of high power density microfluidic fuel cells without lengthy and expensive physical tests.

The first part of this thesis is a numerical analysis of a microfluidic fuel cell consisting of a Y-shaped microchannel in which fuel and oxidant flow in parallel in the laminar regime. The system considered here is based on the design of Choban et al. and a theoretical model is deduced to demonstrate flow kinetics, species transport, and electrochemical reactions at the electrodes with appropriate boundary conditions. A detailed three-dimensional numerical simulation is performed to give physical insights for the characteristics of cell performance and provide a helpful guide to develop the computational model for the next step.

After built up the theoretical model, based on the model and the results generated, a numerical analysis of a microfluidic fuel cell will be conducted. Computational fluid dynamics (CFD) is an essential tool for numerical analysis on microfluidic process. In contrast to macroscale fluid mechanics where there are challenges in modeling turbulence, the main challenges in CFD modeling of microflows lie in the application of appropriate boundary conditions and in modeling species transport. A computational model was employed by COMSOL® to analyze a Y-shaped microfluidic fuel cell with side-by-side streaming. The multidimensional nature of the flow requires a 3D solution using a computational fluid dynamics framework coupled flow, species transport and electrochemical models for both anode

and cathode. The model accounts fully for three-dimensional convective transport in conjunction with anodic and cathodic reaction kinetics. Appropriate boundary conditions for the CFD modeling of this system are developed and applied in the numerical model. The results provide insight into the running parameter, and both microchannel and electrode geometries required to achieve significantly improved performance. Finally, a numerical simulation will be used to guide the microchannel geometry design process, and electrodes as well.

Chapter 2

PRESENT STATUS OF MICROFLUIDIC FUEL CELL MODELING

Fuel cell mathematical modeling is helpful for developers with such advantages as improvement in their design, enhancement of cost efficiency, as well as both quantitative and qualitative improvement of the fuel cells generated. The model must be robust and accurate and be able to provide quick solutions to fuel cell problems. A good model should be able to predict fuel cell performance under a wide range of operating conditions. Even a modest fuel cell model will have large predictive power. A few important parameters like the cell, fuel and oxidant temperatures, the fuel or oxidant pressures, the cell potential, and the weight fraction of each reactant must be solved for in the mathematical model. Instead of conducting several complicated experiments, we can easily improve the performance of fuel cells by modifying all those important parameters, as well as changing the design, materials, and achieving optimization. As soon as we obtain an optimized model, we can start the experiments with the

design of model from our simulation and compare the results between the realistic experiment and the ideal simulation.

There are various commercially available modeling software that have been successful in modeling microfluidics processes, such as Fluent® (http://www.fluent.com), COMSOL® (http://www.comsol.com), CFD-ACE+® from the CFD Research Corporation® (http://cfdrc.com) and Coventor® (http://www.coventor.com). While these excellent tools do present the path of least resistance for high-level numerical analysis, they do in general require the user to acquire some background knowledge in computational fluid dynamics. In addition, many of these software packages tend to be focused primarily on simulation of fluid flow and to a lesser extent, species transport, which as mentioned above does not provide a complete picture of what is required to engineer a true microfluidic system. The multiphysics capabilities of COMSOL® , which facilitates the coupling and simultaneous solution of different fundamental equations along with its point and click interface, make it likely to be the best candidate of the widely available tools for comprehensive modeling. Moreover, some research groups have developed their own software besides these commercial packages, which allow them to be specialized for microfluidic system development.

Since Choban et al.(*8*) firstly demonstrated the membraneless fuel cell using formic acid and oxygen as reactants, this new type of fuel cell also known as microfluidic fuel cell has been rapidly developed not only by several modeling cases(*3*, *7*, *9*)which are based on numbers of numerical study(*10*–*14*), but also in manufacture field(*15*–*19*). They demonstrated that when two streams are flowing in parallel as laminar flow, the streams remain separated, eliminating the need of membrane. Later, they reported a Y-shaped microfluidic fuel cell system(*4*), from those preliminary results, they showed that the fuel cell performance is limited by the transport of reactants through the concentration boundary layer to the elec-

trodes and by the low concentration of oxidant in the cathode stream especially, better ionic conductivity and new channel designs will be helpful for the improvement in the performance.

Before the demonstration of microfluidic fuel cell by Choban et al.(*8*), there were plenty of theoretical research about laminar flow in microchannel, some of which were involved with fluid mechanics, such as the work done by Ismagilov et al.(*12*). It showed that decreasing the channel height while keeping other parameters constant can decrease not only the P*é*clet number and make the difference between the diffusion near the top and bottom walls and in the center in the channel less significant, but also the extent of the diffusional broadening $\delta \sim (DHz/U_a)^{1/3}$ (here D is the diffusivity, H is the height of the channel, z is the distance the fluid flows downstream, and U is the average flow speed.) near the top and bottom walls in the high-P*é*clet-number limit; Some of them are involved with electrochemical reaction. For example, Compton et al.(*11*) used the backwards implicit (BI) method to illustrate, under steady-state conditions, of complex electrode reaction mechanisms pertaining coupled homogeneous kinetics and several kinetic species, which occurred at channel electrodes.

Successively, Lee et al., Phirani and Basu, Chen and Chen, Chen et al.(*10*, *13*, *14*, *20*) conducted several theoretical studys about microfluidic fuel cell. Chen and Chen(*14*) demonstrated a two-dimensional model of microfluidic fuel cell model by using the spectral method where the eigenvalues are obtained by employing Galerkin methods. The similarity transform was adopted to separate the concentrations of the oxidant and the intermediate product from their coupled boundary conditions. As is shown by the results, the limiting average current density increases with the stoichiometry coefficient from electrons in the case of no intermediate product, yet the maximum electric power is independent of this coefficient. By giving the concentrations of the oxidant and the intermediate product at the inlet end

of the cell, they can obtain a condition with increasing the current density. A optimization research of microfluidic fuel cell had been demonstrated by Lee et al.(*10*), it presented theoretical and experimental work to describe the role of flow rate, microchannel geometry, and location of electrodes within a microfluidic fuel cell on its performance by using transport principles. The results showed that the performance of fuel cell can be improved when the electrodes used in designing the device are smaller than a critical length. Besides, Phirani and Basu(*13*) improved the fuel utilization by altering the design of the microfluidic fuel cell. In the study, by introducing a third stream containing sulfuric acid between the fuel and oxidant stream, it enhanced fuel utilization with an increase from 14.1% to 16%.

On a basis of such theoretical work reported above, some recent modeling works came out after. Before the modeling work on microfluidic fuel cell, there were an amount of modeling work on PEM(Proton exchange membrane) fuel cell (*21*–*24*), which are significantly conducive to the micrfluidic fuel cell modeling. Lu and Reddy(*21*) combined the experimental and modeling methods to investigate effects of different factors on the performance of the micro-PEM fuel cell, which is similar to the micrfluidic fuel cell in most of such factors as contact resistance, overpotential, and the dimension of the channel. The results showed that species transport and contact resistance determined the performance of the micro-PEMFC, hence, the designs of new flow field configurations and assembling modes of micro-PEMFCs play a crucial role in improving the performance of micro-PEMFCs. These designs including flow field and assembling mode of micro-PEMFCs are supposed to improve species transport through microchannels and decrease the contact resistance between gas diffusion layers (GDLs) and current collectors. Mann et al.(*22*) demonstrated a theoretical research about the application of Butler-Volmer equations in the modelling of activation polarization for PEM fuel cells, which is also applicable to microfluidic fuel cell. For the reason that fuel cell models must be

capable of predicting values of the activation polarization which depends on the inverse of the electrochemical reaction rate at that electrode interms of Butler-Volmer equations at both the anode and the cathode, this work summarized the important theoretical background, primarily based on the Butler-Volmer equation, which is common to the development of modelling capability for both anode and cathode activation polarization terms in any fuel cell. Cheddie and Munroe(*23*) developed a three dimensional mathematical model of a PEM fuel cell equipped with a PBI membrane, which involved transport phenomena and polarization effects of the fuel cell. It predicted that the greatest area of oxygen depletion occur in the cathode catalyst layer just under the ribs. This depletion increases in the direction of flow, and is more prominent at lower supply gas flow rates. Al-Baghdadi and Al-Janabi(*24*) conducted an optimization study of a PEM fuel cell that incorporates the significant physical processes and the key parameters affecting fuel cell performance by using a comprehensive three-dimensional, multi-phase, non-isothermal model. This model featured an algorithm that gives a more realistic reflection of the local activation overpotentials, which leads to improved prediction of the local current density distribution. This comprehensive model accounts for the major transport phenomena in a PEM fuel cell: convective and diffusive heat and mass transfer, electrode kinetics, transport and phase change mechanism of water and potential fields. All these work can be also applied in microfludic fuel cell modeling.

The first integrated computational study of microfluidic fuel cell based on a T-shaped channel, a concise eletrochemical model of the key reactions and with appropriate boundary conditions is done by Bazylak et al. (*7*) in conjunction with the development of a computational fluid dynamic (CFD) model of this system that accounts for coupled flow, species transport and reaction kinetics. By combing hydrodynamic and mass transport model, and reaction model, which represent mass, momentum and species conservation, and electrochemical kinetics respec-

tively, Bazylak et al. built several three-dimensional microfluidic fuel cell models with different aspect ratios of channel cross section, but adopting the same hydraulic diameter. Then it comes to explain why the reactants demonstrate the least percentage of mixing and the best fuel utilization at the outlet of the fuel cell. The reason is that the rectangular geometry with a correspondingly high aspect ratio in the cross-stream direction is the most promising design for the microfluidic fuel cell, which can effectively decrease the limitation on the performance of the cell caused by the mass transport of reactants through the concentration boundary layers to the electrodes. In addition, lowering the inlet velocity and tailoring the electrode shape design can also enhance fuel utilization.

Yoon et al.(*25*) presented a microfluidic fuel cell model by Comsol®, and with the simulation they figured out three methods to improve the performance of pressure-driven laminar flow-based microreactors by manipulating reaction-depletion boundary layers to overcome mass transfer limitations on the surface of electrodes. In his work, by coupling the Navier-Stokes equations, the continuity equation, the mass conservation equation, and within a boundary condition at the electrode, the Butler-Volmer equation, the model has been built to reduce or even overcome mass transfer limitations resulting from the presence of a depletion boundary layer on the reactive surface which can significantly improve the performance of microfluidic fuel cell.

Chang et al. (*3*) demonstrated a microfluidic fuel cell model containing the flow kinetics, species transport, and electrochemical reactions within the channel and the electrodes is developed with appropriate boundary conditions and solved by a commercial CFD package. Compared to those works that have been done before, the analysis of the cell's performance is been focused on modifying some important physical factors, such as volumetric flow rate, P*é*clet number, as well as and the geometric effect of the size of the channel. Results show that a higher P*é*clet number

can help to improve the cell performance by enhancing electrocatalytic activity on cathode surface since the performance is mainly restricted by the low concentration of oxygen in cathodic stream, also to prevent the fuel crossover as the result of the mixing between the fuel and oxidant streams. On the other hand, for a fixed aspect ratio and volumetric flow rate, a reduction of cross-sectional area will help to achieve higher performance. Additionally, higher oxygen concentration can help to improve the performance as well.

Chapter 3

THEORY

In principle, a microfluidic fuel cell operates like a battery. Unlike a battery, a microfluidic fuel cell does not run down and does not require recharging. It will produce energy in the form of electricity and heat as long as fuel is supplied. In this chapter, multiple disciplines which are involved in microfluidic fuel cell science and technology will be introduced, including microfluidic dynamics, transport phenomena, electrochemistry. Because of the diversity and complexity of electrochemical and transport phenomena contained in a microfluidic fuel cell, before we start the microfluidic modeling and simulation, we have to understand all aspects of the theory.

3.1 Hydrodynamics

3.1.1 Flow Regions

The transport properties of a channel flow depends greatly on the flow region, i.e. developing or developed, and type, i.e. laminar or turbulent. The hydrodynamic

entrance region is where the velocity boundary layer, the pressure gradient, and wall shear stress are developing together and the entrance length is the distance to attain their constant conditions i.e. fully developed conditions. However, the varying asymptotic approaches of the three variables to their constant conditions make it difficult to decide the entrance length precisely. Although the definition of the entrance length can be made in several ways depending on the variable being compared along the channel and the criteria, for engineering purposes, it is defined customarily as the axial distance from the channel entrance required for the centerline velocity to reach 99% of the fully developed centerline velocity.

There are two distinct regions of flow in microfluidic fuel cells' microchannel: the entrance region and the regular flow region. When the fluid enters the channel, the flow (velocity) profile changes from flat to a more rounded and eventually to the characteristic parabolic shape. Once this occurs, it is in the fully developed region of flow, as shown in Figure 3.1 (*26*).

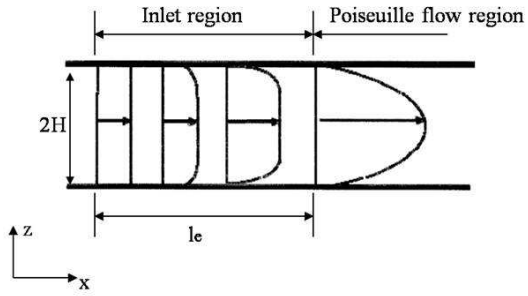

Figure 3.1: Establishment of a Poiseuille profile for a laminar flow in a microchannel.(*1*)

The parabolic profile is typical of laminar flow in channels, and is caused by the existence of the boundary layer. When the fluid first enters the channels, the velocity profile will not yet be parabolic. Instead, this profile will develop over a distance called the entrance length, L_e. L_e depends on the Reynolds number Re and the aspect ratio h/w of the channel. To identify L_e, the parameter $\rho\mu$ is studied on the centerline of the microchannel. In the work of Matteo Martinelli and Vladimir

Viktorov(9), a flow with the parameter $\rho\mu$ that is 97% of the fully developed value is considered to be a full-laminar developed flow. Figure 3-2 shows the parameter $\rho\mu$ versus the length of the microchannel L with the aspect ratio $h/w = 1$ and the Reynolds number Re ranging from 100 to 2100.

The following formula, describing L_e, with a maximum error of 4%, is obtained from numerical results:

$$\frac{L_e}{h} = [-0.129(\frac{h}{w})^2 + 0.157\frac{h}{w} + 0.016\frac{h}{w}]Re \tag{3.1}$$

When the aspect ratio h/w decreases, the fully developed laminar flow will exhibit velocity with a uniform velocity profile. In particular, for $h/w < 0.5$ velocity starts to have a uniform profile and for $h/w < 0.1$ the uniform velocity profile is 90% of the total width of the channel, and flow can be approximated to a 2D flow.

3.1.2 Mass and Momentum Conservation

In a general microfluidic fuel cell device, the Reynolds Number of the flow in the channel is low ($Re < 2300$). In a low Reynolds Number, the flow is laminar, by applying Navier-Stokes equations for momentum conservation in 3-Dimensional incompressible Newtonian fluid, we can easily obtain the velocity field. In this work, the fluid should be treated as a continuum, and this assumption is usually valid in microscale liquid flows, a reasonable accuracy should be applied into the nanofluidic range. Therefore, after applying aforementioned assumptions, the nonlinear convective terms of Navier-Stokes equations can be safely neglected at very low Reynolds numbers, the predictable Stokes flow can be obtained as following:

$$\rho\frac{\delta u}{\delta t} = -\nabla p + \mu\nabla^2 u + f \tag{3.2}$$

where p represents pressure and f summarizes the body forces per unit volume. Furthermore, mass conservation for fluid flow obeys the continuity equation:

$$\frac{\delta\rho}{\delta t} + \nabla\cdot(\rho u) = 0 \tag{3.3}$$

The incompressible condition is applied since the fluid density is constant. For a simple geometry such as parallel plates, or a cylindrical tube,equation 3.2 and equation 3.3 will generate the familiar parabolic pressure-driven velocity profile. However for our geometry design, which is three dimensional channel with rectangular cross section, needs to have a further discussion is needed.

The characteristic of microfluidic flows offers not only good control over fluid-fluid interfaces but also significant functionality. When two liquid streams with similar viscosity and density come into a single microchannel, a parallel co-laminar flow is formed. In this micrfluidic flow, the mass transport contains three terms: convection, diffusion, and electromigration. In general, the electromigration term is neglected since there is sufficient supporting electrolyte, mixing between two co-laminar streams takes place only by transverse diffusion. The Péclet numbers ($Pe = UD_h/D$) in microscale devices are usually high, which indicate that the velocity of mass transfer via stream convective is much higher than transverse diffusion rate, therefore, the diffusive mixing zone is confined in a thin interfacial width at the center of the microchannel. In the cross section view, the interdiffusive mixing zone has an hourglass shape width maximum width (δx) at the channel bottom and top, and this width is given by the following equation:

$$\delta_x \propto (\frac{DHz}{U})^{1/3} \tag{3.4}$$

where D represents the diffusion coefficient, z is the downstream position, and H is the height of the channel. Equation 3.4 is limited by similar streams density,

however, when two liquids have different densities, a gravity-induced reorientation of the co-laminar liquid-liquid interface can occur(*27*).

3.2 Determination of the Velocity Profile

As discussed above, in a tube, after the entrance zone, the flow will get fully developed. Generally, we assume that after the fully developed zone, the flow in the microchannel is laminar since the Reynolds number is low ($Re << 1$), after applying the steady state in the incompressible Stokes equation , neglect the body force(*1*) we have:

$$\nabla \cdot u = 0 \tag{3.5}$$

$$0 = -\frac{1}{\rho}\nabla P + \nabla^2 \cdot (\upsilon u) \tag{3.6}$$

where ρ denotes density ($kg \cdot m^{-1}$), u the velocity vector ($m \cdot s^{-1}$), ν denotes kinematic viscosity ($m^2 \cdot s^{-1}$), and P pressure (Pa).

For equation 3.6, since velocity is a function of y and z, it can be rewritten as:

$$-\frac{\Delta P}{\mu L} = [\delta_y{}^2 + \delta_z{}^2] \cdot v_x(y,z) \tag{3.7}$$

For our case, we have a rectangular cross section microchannel as below:

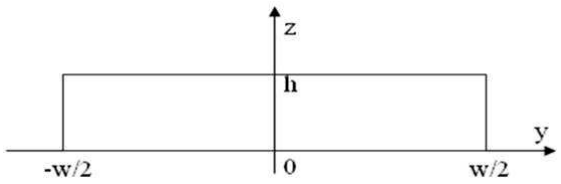

Figure 3.2: The definition of rectangular channel cross section

The Navier-Stokes equation and associated boundary conditions are:

$$-\frac{\Delta P}{\mu L} = [\delta_y{}^2 + \delta_z{}^2]\cdot v_x(y,z), \qquad \text{for } -\frac{1}{2}w < y < \frac{1}{2}w, 0 < z < h,$$
$$v_x(y,z) = 0, \qquad \text{for } \quad y = \pm\frac{1}{2}w, z = 0, z = h, \tag{3.8}$$

There is already a solution presented by Bruus (*1*), which introduces a Fourier series. The detail for this solution can be found in Theoretical Microfluidics (*1*).

The solution $f_n(y)$ that satisfies the no-slip boundary conditions $f_n(\pm\frac{1}{2}w) = 0$ is

$$f_n(y) = \frac{4h^2\Delta P}{\pi^3\mu L}\frac{1}{n^3}[1 - \frac{\cosh(n\pi\frac{y}{h})}{\cosh(n\pi\frac{y}{2h})}], \text{ for n odd,} \tag{3.9}$$

which leads to the velocity field for the Poiseuille flow in a rectangular channel,

$$v_x(y,z) = \frac{4h^2\Delta P}{\pi^3\mu L}\sum_{n,odd}^{\infty}\frac{1}{n^3}[1 - \frac{\cosh(n\pi\frac{y}{h})}{\cosh(n\pi\frac{y}{2h})}]\sin(n\pi\frac{z}{h}). \tag{3.10}$$

The Figures 3.3 below show plots of the contours of the velocity field and of the velocity field along the symmetry axes.

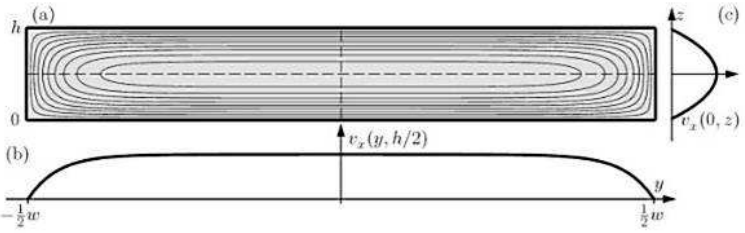

Figure 3.3: (a) Contour lines for the velocity field $v_x(y,z)$ for the Poiseuille-flow problem in a rectangular channel. The contour lines are shown in steps of 10% of the maximal value$v_x(0,h/2)$. (b) A plot of $v_x(y,h/2)$ along the long centerline parallel to e_y. (c) A plot of $v_x(0,z)$ along the short centerline parallel to e_z.(*1*)

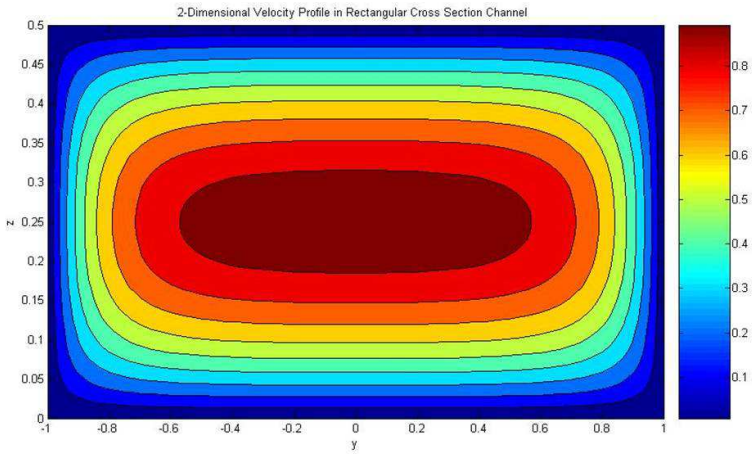

Figure 3.4: 2-Dimensional Velocity Profile in Rectangular Cross Section Channel.

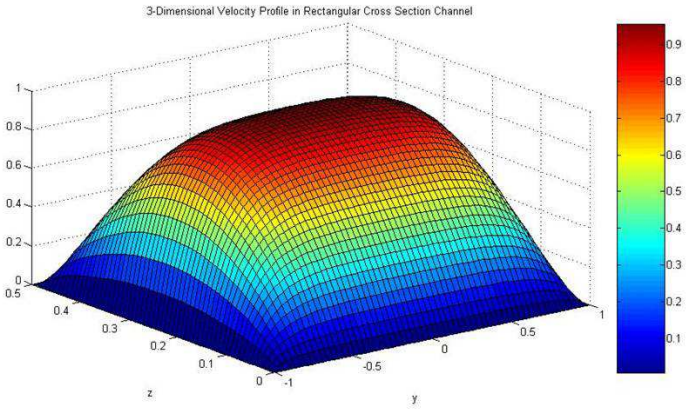

Figure 3.5: 3-Dimensional Velocity Profile in Rectangular Cross Section Channel.

After solving the equation 3.10 in Matlab®, we have the 2-D and 3-D velocity profiles below:

3.3 Mass Transfer

In order to produce electricity, a fuel cell must be supplied continuously with fuel. In addition, the produced water must be removed continually to maintain high fuel cell efficiency. Voltage losses occur in the fuel cell due to activation losses, ohmic losses, and mass transport limitation-which is the topic of this section. Mass

transport is the study of the flow of species, and can significantly affect fuel cell performance. Losses due to mass transport are also called "concentration losses," and can be minimized by optimizing mass transport in the flow field plates, diffusion layers, and catalyst layers. This section covers both the macro and micro aspects of mass transport.

After solving the Navier-Stokes equations, we come to the transport equations which are complicated with chemical processes occurring heterogeneously (i.e. at the electrode surface; electrochemical reaction) or homogeneously (in the solution; chemical reaction). In many cases of microfluidics, where the flow velocities are much smaller than the velocity of pressure waves in the liquid, the fluid can be regarded as incompressible.

The general transport components are all included in the general Nernst-Planck equation for the flux J_i of species i, which shows in Equation 3.11 (*28*)

$$J_i = -D_i \nabla C_i - \frac{z_i F}{RT} D_i C_i \nabla \phi + C_i v, \tag{3.11}$$

in which J_i is the molar flux per unit area of species i at the given point in space, D_i the species diffusion coefficient, C_i its concentration, z_i its charge, F, R and T have their usual meanings, ϕ is the potential and v the fluid velocity vector of the surrounding solution. For solutions containing an excess of supporting electrolyte, the ionic migration term can be neglected 3.11; we will assume this to be the case in our study. The velocity vector, v, represents the motion of the solution and is given in Cartesian coordinates by,

$$v(x, y, z) = iv_x + jv_y + kv_z, \tag{3.12}$$

where i, j and k are unit vectors, and v_x, v_y and v_z are the magnitudes of the solution velocities in the x, y and z directions at point (x, y, z). Similarly, in Cartesian

coordinates,

$$\nabla C_i = gradC_i = i\frac{\delta C_i}{\delta x} + j\frac{\delta C_i}{\delta y} + k\frac{\delta C_i}{\delta z}. \tag{3.13}$$

The variation of C_i with time is given by

$$\frac{\delta Ci}{\delta t} = -\nabla J_i. \tag{3.14}$$

By combining equation 3.11 and equation 3.13, assuming that migration is absent and that D_j is not a function of x, y and z, we obtain the general convective-diffusion equation:

$$\frac{\delta C_j}{\delta t} = D_j\nabla^2 C_j - v\cdot\nabla C_j. \tag{3.15}$$

Note that in the absence of convection (i.e. $v = 0$), equation 3.15 is reduced to diffusion equations. Before the convection-diffusion equation can be solved for the concentration profiles, $C_i(x, y, z)$ and subsequently for the currents from the concentration gradients at the electrode surface, expressions for the velocity profile, $v(x, y, z)$, must be obtained in terms of x, y and z.

Previously, we already got the velocity field of the Poiseuille flow in a rectangular cross section microchannel as equation 3.10. When a steady velocity profile has been attained like Poiseuille flow, the concentrations near the electrode are no longer functions of time,$\frac{\delta C}{\delta t}$, and the steady state convective-diffusion equation (5), written in terms of Cartesian coordinates, becomes

$$v_x(\frac{\delta C}{\delta x}) + v_y(\frac{\delta C}{\delta y}) + v_z(\frac{\delta C}{\delta z}) = D[\frac{\delta^2 C}{\delta x^2} + \frac{\delta^2 C}{\delta y^2} + \frac{\delta^2 C}{\delta z^2}]. \tag{3.16}$$

Assuming diffusion in the direction of the convection flow (i.e. $\frac{\delta^2 C}{\delta x^2} = 0$) to be negligible,$v_y = v_z = 0$, so the equation 3.16 will be:

$$\{\frac{4h^2\Delta P}{\pi^3 \mu L}\sum_{n,odd}^{\infty}\frac{1}{n^3}[1-\frac{\cosh(n\pi\frac{y}{h})}{\cosh(n\pi\frac{y}{2h})}]\sin(n\pi\frac{z}{h})\}(\frac{\delta C}{\delta x}) = \frac{\delta^2 C}{\delta y^2}+\frac{\delta^2 C}{\delta z^2}. \tag{3.17}$$

3.4 Electrochemistry

A fuel cell is an electrochemical energy converter. Its operation is based on the following electrochemical reactions happening simultaneously on the anode and cathode, in the case of a hydrogen fuel cell:

At the anode:

$$H_2 \rightarrow 2H^+ + 2e^- \tag{3.18}$$

At the cathode:

$$\frac{1}{2}O_2 + 2H^+ + 2e^- \rightarrow H_2O \tag{3.19}$$

Overall:

$$H_2 + \frac{1}{2}O_2 \rightarrow H_2O \tag{3.20}$$

More precisely, the reactions happen on an interface between the ionically conductive electrolyte and electrically conductive electrode which been deposited by catalyst.

The maximum amount of electrical energy generated in a fuel cell corresponds to Gibbs free energy, ΔG, of the above reaction:

$$W_{el} = -\Delta G. \tag{3.21}$$

The theoretical potential of fuel cell, E, is then:

$$E = \frac{-\Delta G}{nF}, \tag{3.22}$$

where n is the number of electrons involved in the above reaction, and F is Faraday´s constant (96,485 Coulombs/electron-mol). Since ΔG, n and F are all known, at 25°C and atmospheric pressure, the theoretical hydrogen oxygen fuel cell potential can be calculated by:

$$E = \frac{-\Delta G}{nF} = \frac{237,340}{2 \cdot 96,485} \frac{Jmol^{-1}}{Asmol^{-1}} = 1.23 Volts. \tag{3.23}$$

Assuming that all of the Gibbs free energy can be converted into electrical energy, the maximum efficiency of a fuel cell that can be achieved (theoretically) is a ratio between the Gibbs free energy and hydrogen higher heating value, ΔH:

$$\eta = \Delta G / \Delta H = 237.34/286.02 = 83\% \tag{3.24}$$

Actual cell potentials are always smaller than the theoretical ones due to inevitable losses. Voltage losses in an operational fuel cell are caused by several factors such as:

- kinetics of the electrochemical reactions (activation polarization),
- internal electrical and ionic resistance,
- difficulties in getting the reactants to reaction sites (mass transport limitations),
- internal (stray) currents,
- crossover of reactants.

3.4.1 Electrode Kinetics

We first start with ohmic drop, which is caused by the electric resistance of the electrolyte, R_{elt}; in general, the ohmic drop is proportional to I.

Overpotential (η) is existing at both the anode and cathode; It is generally proportional to log I, and is not rate-determining.

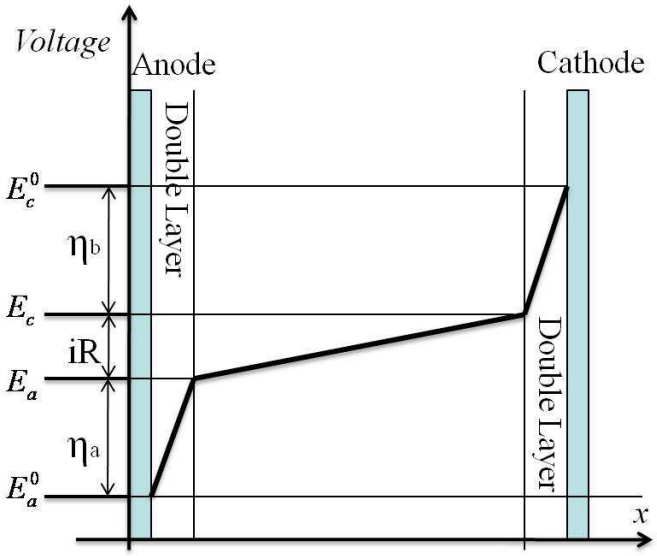

Figure 3.6: Overpotential on the electrodes

This Figure 3.6 below is only approximate. During operation, the electrolyte resistance can change as a result of temperature changes or changes in electrolyte composition and concentration, especially near the electrode. On the other hand, η_a and η_c are logarithmic functions of the current. For a simple cathode reaction,

$$Ox + ne^{-1} \rightleftharpoons Red \tag{3.25}$$

the following (again simplified) relations apply:

$$I = nFk^{o\prime}[c^*_{Red} exp\{\alpha_a nf(E - E^o)\} - c^*_{Ox} exp\{-\alpha_c nf(E - E^o)\}] \tag{3.26}$$

or

$$I = I_0[exp(\alpha_a n f \eta) - exp(-\alpha_c n f \eta)] \tag{3.27}$$

with

$$I_0 = nFk^{o\prime}(c^*_{Ox})^{\alpha_a}(c^*_{Red})^{\alpha_c} = I^o_0(c^*_{Ox})^{\alpha_a}(c^*_{Red})^{\alpha_c} \tag{3.28}$$

and

$$\eta = a + b \log |I| \tag{3.29}$$

with the Tafel slope

$$b = \frac{\partial \eta}{\partial \log |I|} \tag{3.30}$$

In these equations (2), n, F, E, and E^o have their usual meaning. $k^{o\prime}$ is the standard heterogeneous rate constant ($m^3 \cdot s^{-2}$); c_{Red}, c_{Ox} represent the concentrations ($mol \cdot dm^{-3}$) of the reductant and the oxidant, with the degree symbol representing the concentration at the phase boundary, and the asterisk the concentration in the bulk of the solution, respectively.

$$f = \frac{F}{RT} \tag{3.31}$$

I_0 is the exchange current density in $A \cdot m^{-2}$; I^o_0 is standard I_0; α_a, α_c are the transition coefficients for the anodic and cathodic processes, respectively; $\alpha_a = 1 - \alpha$ and $\alpha_c = \alpha$; and $\eta = E - E_{eq}$, i.e., the difference between the actual and the equilibrium E values ($E_{eq} = E$ at $I = 0$); see Figure 3.6.

As soon as the fuel cell reaction starts, the concentrations of reductant and oxidant in the immediate vicinity of the anode, c^o_{Red}, and the cathode, c^o_{Ox}, respectively, decrease and new reactants are supplied by diffusion. In general, diffusion helps determine the rate; moreover, the diffusion (and so the current) is governed by Fick's law:

$$I_i = nF \cdot D_i(c_i^* - c_i^o)/\delta_N, \tag{3.32}$$

with the subscript i representing species i, D_i the diffusion coefficient ($m^2 \cdot s^{-1}$), and the δ_N so-called Nernstian diffusion layer.

By calculating, the concentration gradient $(c_i^* - c_i^o)/\delta N$ approaches a maximum value and so does the current for $c_i^o \to 0$. In that case $I \to I_d$, and I_d is the diffusion current. From equation 3.32, it can easily be derived that $I \sim c^* - c^o$, and so $I_d \sim c^*$.

Equations 3.26 to 3.28 are valid when the diffusion rate is infinite, which is rarely true. If diffusion is also rate-determining, then the aforementioned equations must be transformed to

$$I = nFk^{o\prime}[c_{Red}^o exp\{\alpha_a nf(E - E^o)\} - c_{Ox}^o exp\{-\alpha_c nf(E - E^o)\}] \tag{3.33}$$

$$I = I_0[\frac{c_{Red}^o}{c_{Red}^*} exp\{\alpha_a nf\eta\} - \frac{c_{Ox}^o}{c_{Ox}^*} exp(-\alpha_c nf\eta)] \tag{3.34}$$

From a didactic point of view, equation 3.33 and equation 3.34 are easier to handle: the exchange current (density), I_0, is a direct measure of the electrode reaction rate; a high value means that the reaction proceeds rapidly, or as called in the electrochemical reversibly.

This is known as the Butler-Volmer equation. Note that the equilibrium potential at the fuel cell anode is $0V$, and the reversible potential at the fuel cell cathode is $1.229V$ and it does vary with temperature and pressure.

Since the ration proceeds in both directions simultaneously, at equilibrium, the net current is zero at equilibrium, we still envision balanced faradaic activity that can be expressed in terms of the exchange current, I_0, which is equal in magnitude to either component current, I_c or I_a.

$$I_o = nFk_b^o c_{Red}^o exp[-\alpha_a nfE_r] = nFk_f^o c_{Ox}^o exp[-\alpha_c nfE_r] \tag{3.35}$$

The exchange current density is the measurement of the readiness of the electrode to proceed with the chemical reaction, which depends critically on the nature of the electrode, besides it is also a function of temperature, catalyst loading, and catalyst-specific surface area. Therefore, when the exchange current density gets higher, the electrons get easier to shift, and the surface of electrode gets more active.

When the exchange current is very large, the system supplies large currents, accompanying with insignificant activation overpotential. However, when the exchange current is low, no significant current flows can be supplied, in this case, a large activation overpotential need to be applied. For charge exchange across the interface, the exchange current can be viewed as a kind of "idle current", and only a tiny overpotential will be required to obtain a net current that is only a small fraction of this idle current. If we need for a net current that is higher than the exchange current, we have to deliver charge at the required rate by applying a significant overpotential. Therefore, exchange current is a measure of any system's ability to deliver a net current without a significant energy loss due to activation.(*26*).

3.4.2 Cell Potential: Polarization Curve

In the electrochemical reaction process of microfluidic fuel cells system, there are three types of losses as shown in Figure 3.7, and it views the largest losses are the activation losses at all current density.

Since activation and concentration polarization are taking place at both anode and cathode, the cell votage can be presented as following:

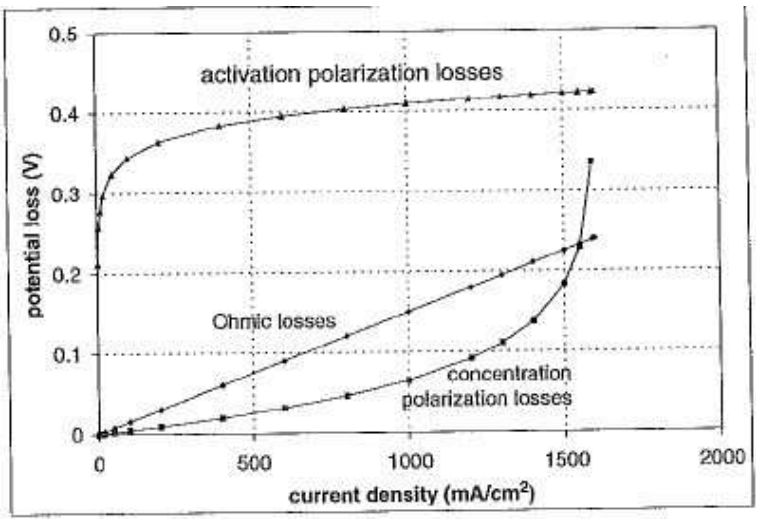

Figure 3.7: Voltage losses in the fuel cell (*2*)

$$V_{cell} = E_r - (\Delta V_{act} + \Delta V_{conc})_a - (\Delta V_{act} + \Delta V_{conc})_c - \Delta V_{ohm} \tag{3.36}$$

Figure 3.6 gives a view of potential distribution in a typical micrfluidic fuel cell over the cell cross section. At open circuit, when there is no current generated, the anode is at reference potential which shown as E_a^0 and the cathode is at the potential corresponding to the reversible potential which shown as E_c^0 at given temperature, pressure, and oxidant concentration. As soon as the current is being generated, the cell potential, measured as the difference between cathode and anode solid phase potentials (solid phase means electrically conductive parts) which shown as $E_c - E_a$, drops because of various losses as discussed earlier.

Note that the cell potential is equal to the reversible cell potential (or the equilibrium potential, E_{eq}) reduced by the potential losses:

$$E_{cell} = E_r - E_{loss} \tag{3.37}$$

where the losses are composed of activation and concentration polarization on both anode and cathode and of ohmic losses as discussed earlier:

$$E_{loss} = \eta_c + \eta_a + \Delta V_{ohm} = (\Delta V_{act} + \Delta V_{conc})_a + (\Delta V_{act} + \Delta V_{conc})_c + \Delta V_{ohm} \tag{3.38}$$

The cell potential is equal to the difference between the cathode and the anode solid state potentials:

$$E_{cell} = E_c - E_a \tag{3.39}$$

where the cathode potential is:

$$E_c = E_c^0 - \eta_c = E_c^0 - (\Delta V_{act} + \Delta V_{conc})_c \tag{3.40}$$

and the anode potential is:

$$E_a = E_a^0 - \eta_a = E_a^0 - (\Delta V_{act} + \Delta V_{conc})_a \tag{3.41}$$

All these potentials may be tracked down in Figure 3.6.

3.4.3 Voltage Losses

As mentioned above, in a microfluidic fuel cell, there are different kinds of voltage losses caused by several factors, such as kinetics of the electrochemical reactions, internal electrical and ionic resistance, internal currents and also crossover of reactants. Besides, the operating conditions such as temperature, applied load, and fuel/oxidant flow rates also lead to voltage losses. The three major classifications of losses that result in the drop from open-circuit voltage are (1) activation polarization, (2) ohmic polarization, and (3) concentration polarization.

Activation polarization is a polarization due to charge transfer kinetics of the electrochemical process involved, and also associated with sluggish electrode kinetics. The higher the exchange current density is, the lower the activation polarization losses are. These losses take place at both anode and cathode; however, since oxidant reduction is a much lower reaction than hydrogen oxidation, it requires much higher overpotentials.

The ohmic overpotential appears as the simple product of a resistance and a current between the anodic and cathodic sites of a fuel cell reaction process, because of resistance to the flow of ions in the electrolyte and resistance to the flow of electrons through the electrode. The total internal resistance of fuel cell includes ionic, electronic, and contact resistance. Electronic resistance is almost negligible, since the material is used for current collectors can hardly be effective. Ionic and contact resistances are approximately of the same order of magnitude.

Concentration polarization is the polarization component which caused by concentration changes in the environment adjacent to the surface of electrodes. When a reactant is rapidly consumed, the mass transport of that reactant close to the surface can become rate controlling. The relationship between the electrochemical reaction potential changes and partial pressure of the reactants can be given by the Nernst Equation.

$$\Delta V = \frac{RT}{nF} ln(\frac{c_b}{c_s}) \tag{3.42}$$

where c_b is the bulk concentration of reactant (mol/cm^3); c_s is the concentration of reactant at the surface of the catalyst (mol/cm^3).

Chapter 4

MODELING

Computational fluid dynamics (CFD) is an essential tool in the development of microfluidic processes. Fuel cell modeling based on CFD is significantly helpful to improve the design of fuel cell, reduce cost, and generate more high-efficient fuel cells. It can quickly provide us a robust and accurate solutions to fuel cell problems, and enables us to predict fuel cell performance under a wide range of fuel cell operating conditions. The necessary improvements in fuel cell performance and operation demand better design, materials, and optimization. These issues can only be addressed if realistic mathematical process models are available.

COMSOL® is a powerful and interactive environment for modeling and solving scientific and engineering problems based on partial differential equations. With some modifications, it can extend conventional models that address one branch of physics to multiphysics models that simultaneously involve multiple branches of science and engineering, sequentially, providing a platform to combine fluid and electrochemical problems in one model.

The set of governing equations presented in chapter 3 have been all solved using COMSOL® Multiphysics 3.5. This chapter is designed to give some background information on the commercial software and how it has been utilized in order to solve the problems at hand for this thesis.

4.1 Layout of Model Development

In this chapter, a comprehensive three dimensional microfluidic fuel cell model has been developed at the end, before that, in order to have an exhaustive understanding on building up such model with COMSOL® Multiphysics, there are a test model with respect to electrochemical reaction on electrode associate with species diffusion, and an integral two dimensional model of microfluidic fuel cell are presented respectively, only necessary analysis are given at the end of this two models to validate practicability of COMSOL® modeling on this work. Afterward, for the results of this final three dimensional microfluidic fuel cell model, a systematic analysis are presented, with various comparison of some other simulation and experimental work which have been done.

4.2 Model Description

By understanding the governing equations, we come to the following built-in modules.

- The convection and diffusion equation module is used to solve for the species conservation. The species specified are reductant and oxidant. This module exits in two domains out of four computational domains, and two microchannels. It is set to inactive in the electrodes domain since no reactant specie's transport occurs in the electrodes. It is important to choose oxidant as the

main species, then it is the reductant, since the entire current density cannot increase significantly with the fuel concentration but can be limited obviously by the low oxidant concentration(*4*).

- The AC/DC Module is employed to compute the solid and electrolyte potentials. Two modules are needed to solve for the potentials, one called electronic module, represents the solid potential in the electrodes domain while the other, called ionic module, represents the electrolyte potential in the microchannel domain. They should work independently, which means one would be set to inactive when other is active.

- The incompressible Navier-Stokes equation under the chemical engineering modules used to solve for the momentum conservation and the velocity profile in the channel. Like the convection and diffusion module, for the reason that no reactant specie's transport occurs in the electrodes, it is set to inactive in the electrodes domain.

4.3 Constants and Variables

There are several ways to input necessary information into COMSOL. The constants option is used to define those global parameters which are the same for all geometries and subdomains. One can use constants in any physics settings, expressions, and coupling variables, also one can use them in expressions while postprocessing the solution. The physical and thermal parameters of this work are defined in Tables 4.1.

The scalar expressions option is used to define expression variables that are valid on all geometry levels everywhere in the current geometry.

Table 4.1: Operating and physical conditions

Parameter	Value	Unit
Faraday's constant(F)	96500	$C \cdot mol^{-1}$
Atmospheric pressure(P_{atm})	1	atm
Temperature(T)	25	°C
Gas constant(R)	8.314	$J \cdot mol^{-1} \cdot K^{-1}$
Viscosity of all solutions(μ)	0.001	$Kg \cdot m^{-1} \cdot s^{-1}$
Diffusivity of all solutions(D)	10^{-9}	$m^2 \cdot s^{-1}$
Overpressure in anode inlet(ΔP_a)	2	Pa
Overpressure in cathode inlet(ΔP_c)	4	Pa
Anodic exchange current(i_{0a})	1	$A \cdot m^{-2}$
Cathodic exchange current(i_{0c})	0.1	$A \cdot m^{-2}$
Anode specific surface area(S_a)	10^{-8}	m^{-1}
Cathode specific surface area(S_c)	10^{-8}	m^{-1}
Initial cell polarization(V_{pol})	0.05	V
Anodic equilibrium voltage($\Delta\phi_{eqa}$)	0	V
Cathodic equilibrium voltage($\Delta\phi_{eqc}$)	1	V
Electrolyte conductivity(k_l)	5	$S \cdot m^{-1}$
Current collector conductivity(k_s)	5000	$S \cdot m^{-1}$
Solution density(ρ)	1000	$Kg \cdot m^{-1}$
Anode reference concentration(c_{refa})	200	$mol \cdot m^{-3}$
Cathode reference concentration(c_{refc})	1	$mol \cdot m^{-3}$
Anode inlet concentration(c_{0a})	200	$mol \cdot m^{-3}$
Cathode inlet concentration(c_{0c})	1	$mol \cdot m^{-3}$

4.4 Test Modeling: Cottrell Experiment

4.4.1 Introduction

We started the modeling with a simple two dimensional case about redox reaction on the electrode surface in order to have a basic understanding about COMSOL®. This work, which contains electrochemical reaction and species diffusion in the electrolyte, can help to understand better the microfluidic fuel cell modeling. This model simulates the electrochemical redox reaction on the surface of electrode typically found in electroplating. The purpose of the model is to demonstrate the

coupling transient diffusion module with conductive media DC and to investigate the reactant concentration distribution in terms of time-dependent factor, diffusion layer, and voltammograms.

4.4.2 Statement of the Problem

We consider our simple redox reaction as:

$$Red \Leftrightarrow Ox + ne^{-} \tag{4.1}$$

in the condition of applying a constant potential voltage on the two sides of electrode as $0.2V$. The electrochemical reaction takes place on the surface of the electrode (x=0). The reactants first have to diffuse through the electrolyte in order to be able to proceed to the electron transfer. The situation is controlled by diffusion and heterogeneous kinetics shown in Figure 4.1.

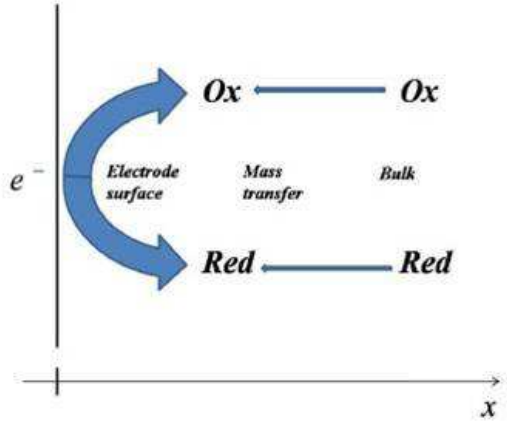

Figure 4.1: Heterogeneous kinetics and diffusion

The diffusion in the electrolyte is described by Fick's laws:

$$\frac{\delta c_{ox}}{\delta t} = D_{ox}\frac{\delta^2 c_{ox}}{\delta x^2}$$
$$\frac{\delta c_{red}}{\delta t} = D_{red}\frac{\delta^2 c_{red}}{\delta x^2} \tag{4.2}$$

At the electrode surface one has (anodic current is positive)

$$j = -nFD_{ox}\frac{\delta c_{ox}}{\delta x}|_{x=0} = nFD_{red}\frac{\delta c_{red}}{\delta x}|_{x=0} \tag{4.3}$$

As initial and boundary conditions we have:

$$t = o, x \geq 0 \qquad c_{red} = c^0_{red}$$
$$t \geq o, x \to 0 \qquad c_{red} = c^0_{red} \tag{4.4}$$

and if we assume that no oxidant is present at the beginning of the experiment:

$$t = o, x \geq 0 \qquad c_{ox} = 0$$
$$t \geq o, x \to 0 \qquad c_{ox} = 0 \tag{4.5}$$

The partial differential equation 4.2 being of second order, we need a second boundary condtion. This second condition depends on the type of reaction being considered and is derived from equation 4.3.

4.4.3 Model Description

The physical domain of the model is a 2-dimensional channel through which the flow is happening is independent on z position, it might be tempting to consider the flow to be two-dimensional. The model geometry is depicted in Figure 4.2.

The right vertical boundary represents the anode, while the cathode is placed at the right side. The horizontal walls correspond to the pattern are assumed to be insulating.

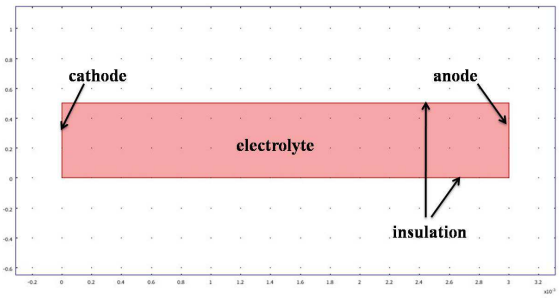

Figure 4.2: Model domain with boundaries corresponding to the anode, cathode, and horizontal insulate walls.

Consider Figure 4.2, showing a long thin tube representing an electrochemical cell, bounded at left end by an electrode which is our focus and filled with electrolyte and an electroactive substance initially at concentration c^*(the bulk concentration). We place the left electrode at $x = 0$ and the other, counter-electrode, at a large distance, we assume as infinite far from the cathode. At $t = 0$, a voltage potential is applied on the two sides of electrodes, such that our electroactive substance reacts at the electrode infinitely fast - that is, its concentration c_0 at the electrode ($x = 0$) is forced to zero and kept there.

As mentioned above, there are transient diffusion modules with conductive media DC coupled together. For the transient diffusion module, where the Fick's equation is applied:

$$\frac{\delta c_i}{\delta t} + \nabla \cdot (-D \nabla c_i) = 0. \tag{4.6}$$

Since there are both reductant and oxidant involved in this reaction, so it has to apply both two species in the subdomains setting. Besides, it also needs to define the diffusion coefficient D, and the initial concentrations of those two species $c_{i(t=0)}$. For the boundary condition setting, we need to define the cathode surface where

the reaction occurred as two fluxes from equation 4.3. The anode side is assumed to be infinitely far away from the cathode, i.e, the concentration of the reactant on the surface is fixed as the bulk concentration while the concentration of the product is zero.

A Conductive Media DC application module describes the potential distributions in the subdomain using the following equations:

$$\nabla \cdot (-k_{l,eff} \nabla \phi_l) = 0. \tag{4.7}$$

Here $k_{l,eff}$ is the effective electronic conductivity (S/m) of the electrolyte. The potential (V) in the electrolyte phases is denoted by ϕ_l. This models the active layer of the two electrodes as boundaries. It means that the charge-transfer current density can be generally described by using the Butler-Volmer electrochemical kinetic expressions as in Equation 4.8, as a boundary condition on the surface of cathode.

$$i_c = i_0\Big(\frac{c_{red}}{c^0_{red}} \exp\frac{0.5F\eta}{RT} - \frac{c_{ox}}{c^0_{ox}} \exp\frac{-0.5F\eta}{RT}\Big) \tag{4.8}$$

where i_0 is the exchange current density (A/m^2), c_{red} and c^0_{red} are the concentration on the surface of electrode and bulk concentration of reductant respectively (mol/m^3), c_{ox} and c^0_{ox} are the concentration on the surface of electrode and bulk concentration of oxidant respectively (mol/m^3). Furthermore, F is Faraday's constant (C/mol), R the gas constant $(J/(mol \cdot K))$, T the temperature (K), and η the overpotential (V); we assumed a symmetry factor of 0.5.

In addition, on the cathode surface, by applying equation 4.3, we have the boundary condition below:

$$-nFD_{ox}\frac{\partial c_{ox}}{\partial x}|_{x=0} = nFD_{red}\frac{\partial c_{red}}{\partial x}|_{x=0} = i_0\Big(\frac{c_{red}}{c^0_{red}} \exp\frac{0.5F\eta}{RT} - \frac{c_{ox}}{c^0_{ox}} \exp\frac{-0.5F\eta}{RT}\Big) \tag{4.9}$$

In other words, we have the boundary condition for both reductant and oxidant on the cathode surface as two fluxes:

$$\frac{\partial c_{ox}}{\partial x}|_{x=0} = -\frac{i_0}{nFD_{ox}}\left(\frac{c_{red}}{c_{red}^0}\exp\frac{0.5F\eta}{RT} - \frac{c_{ox}}{c_{ox}^0}\exp\frac{-0.5F\eta}{RT}\right) \tag{4.10}$$

$$\frac{\partial c_{red}}{\partial x}|_{x=0} = \frac{i_0}{nFD_{red}}\left(\frac{c_{red}}{c_{red}^0}\exp\frac{0.5F\eta}{RT} - \frac{c_{ox}}{c_{ox}^0}\exp\frac{-0.5F\eta}{RT}\right) \tag{4.11}$$

For the anode which is on the other side, we just set the boundary condition as two fixed concentrations which are the bulk concentration for each of them.

4.4.4 Results

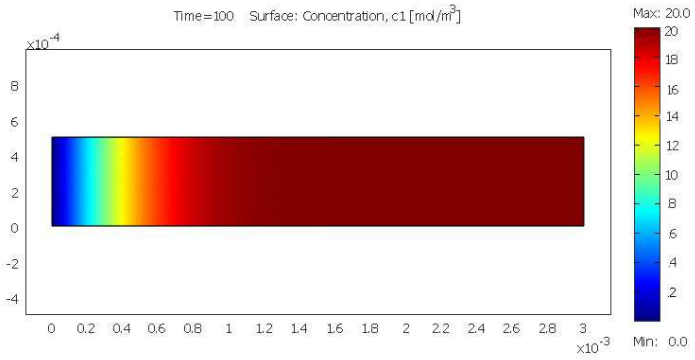

Figure 4.3: Oxidant concentration ($mole/m^3$), current density streamlines in the tube after 100 seconds of operation.

After meshing with a number of degrees of freedom as 9843, 1568 triangular elements, we solve the model with time dependent solver for 100 seconds which is able to give us a full scale set of results.

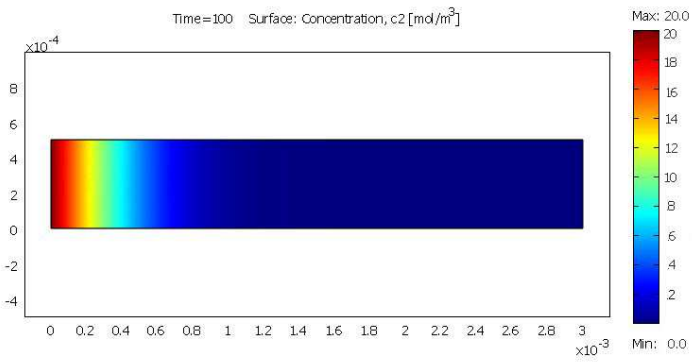

Figure 4.4: Reductant concentration ($mole/m^3$), current density streamlines in the tube after 100 seconds of operation.

Figure 4.3 and Figure 4.4 show the concentration distribution of oxidant and reductant and the current density lines after 100 seconds of operation. The figures clearly show that there are reductants produced on the surface of the cathode and oxidant consumed, demonstrated by the decreasing and increasing of each concentration. In addition, the simulation shows substantial variations in oxidant concentration in the cell. Such variations eventually cause free convection in the cell.

The numerical solution of oxidant concentration from equation 4.10 is shown in Figure 4.5 for four values of t each in black color, increasing as the curves go to the right. The so-called concentration profiles partially agree with our intuitive picture. The analytical solution of the Cottrell experiment (*29*) is known:

$$c(x,t) = c^* erf(\frac{x}{2\sqrt{Dt}}), \tag{4.12}$$

with $c(x,t)$ the concentration of species changing by distance from the electrode x and time t, c^* the initial concentration, and D the diffusion coefficient. The func-

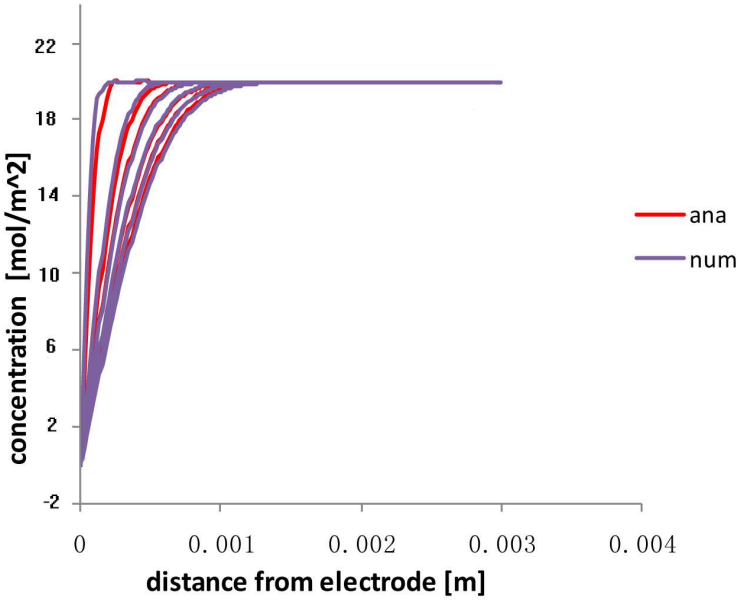

Figure 4.5: Concentration profile changing with time. Analytical solution from error function is presented in red color, and numerical solution from modeling is presented in purple color.

tion erf is the error function, which can be numerically computed. The analytical solution is shown in Figure 4.5 for the three values of t in red color, increasing as the curves go to the right.

Figure 4.5 clearly shows the degree of agreement between the analytical solution from error function and numerical solution from COMSOL ® modeling is excellent.

Aforementioned, this test modeling is a pre-study about understanding how to simulate electrochemical problems in COMSOL Multiphysics® by Cottrell experiment (*29*). In this study, a simple two dimensional diffusion-controlled potential-step model has been introduced, by applying corresponding modules and appropriate boundary conditions, a concentration profile changing with time is obtained in Figure 4.5, it shows that this modeling work has a excellent response for the analytical solutions after certain distance away from electrode, which make it confident enough to start modeling our microfluidic fuel cell by using COMSOL Multiphysics®.

4.5 2-Dimensional Model

4.5.1 Model Introduction

In this section, we build a stationary 2-Dimensional model of a microfluidic fuel cell based on a training model in COMSOL Multiphysics ® – Proton Exchange Membrane(PEM) Fuel Cell. This PEM fuel cell model uses current balances, mass transport equations (Maxwell-Stefan diffusion for reactant, water and nitrogen gas), and momentum transport (gas flow) to simulate a PEM fuel cell's behavior. By applying microfluidic fuel cell's condition in the PEM fuel cell model, instead of using Darcy's law module and Maxwell-stefan diffusion and convection module, this model employs incompressible Navier-Stokes module, convection and diffusion module, since the flow in channel is liquid and there's no gas diffusion layer. These four modules help to form a complete fuel cell model. This model simulates the electrochemical reaction on each electrode by Butler-Volmer equations which make it capable to couple with convection and diffusion module, additionally, it simulates the flow by using Navier-Stokes equation. The purpose of this model is to achieve a complete 2-Dimensional microfluidic fuel cell, try to understand the principles of fuel cell modeling, and prepare for the 3-Dimensional case modeling.

4.5.2 Model Definition

As we can see in Figure 4.7, the modeled section of the fuel cell consists of three domains: an anode (Ω_a), a electrolyte flow domain (Ω_e), and a cathode (Ω_c). Two current collectors are located on the top of each electrode. The microchannel has two inlets and two outlets, which are located on the top and bottom respectively.

For the fuel solution, formic acid has been selected, for the reason that it is a small organic molecule fed directly into the fuel cell, removing the need for com-

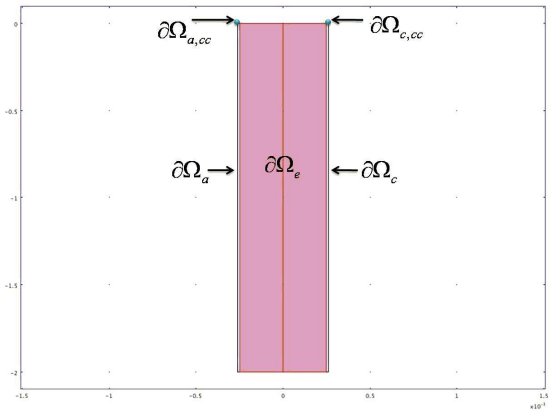

Figure 4.6: 2-D Model geometry with subdomain and boundary labels

plicated catalytic reforming; in addition, storage of formic acid is much easier and safer than that of hydrogen because it does not need to be done at high pressures and (or) low temperatures, as formic acid is a liquid at standard temperature and pressure. Moreover, there are some work have been done with using formic acid that showing a superior power output comparing to hydrogen(*6*). Therefore, the formic acid has been decide as fuel solution in this work with oxygen saturated in the sulfuric acid as the oxidant, are both supplied to the inlet channels of the anode and cathode, respectively. Electrochemical reactions are assumed to take place on the surface of electrodes which are covered by a catalyst layer. The reactions are the following:

At the anode:

$$HCOOH \rightarrow CO_2 + 2H^+ + 2e^- \tag{4.13}$$

At the cathode:

$$\frac{1}{2}O_2 + 2H^+ + 2e^- \rightarrow H_2O \tag{4.14}$$

Overall:

$$HCOOH + \frac{1}{2}O_2 \rightarrow H_2O + CO_2 \tag{4.15}$$

Table 4.2: Operating and physical conditions for 2-Dimensional microfluidic fuel cell

Parameter	**Value**	**Unit**
Faraday's constant(F)	96500	$C \cdot mol^{-1}$
Atmospheric pressure(P_{atm})	1	atm
Overpressure, anode inlet(ΔP_a)	0.25	Pa
Overpressure, cathode inlet(ΔP_c)	0.5	Pa
Temperature(T)	25	°C
Gas constant(R)	8.314	$J \cdot mol^{-1} \cdot K^{-1}$
Viscosity of all solutions(μ)	0.001	$Kg \cdot m^{-1} \cdot s^{-1}$
Diffusivity of catholyte(D_c)	2.1×10^{-9}	$m^2 \cdot s^{-1}$
Diffusivity of anolyte(D_a)	2.546×10^{-9}	$m^2 \cdot s^{-1}$
Anodic exchange current(i_{0a})	0.1194	$A \cdot m^{-2}$
Cathodic exchange current(i_{0c})	3.1×10^{-7}	$A \cdot m^{-2}$
Initial cell polarization(V_{pol})	0.05	V
Anodic equilibrium voltage($\Delta\phi_{eqa}$)	0.2	V
Cathodic equilibrium voltage($\Delta\phi_{eqc}$)	1.23	V
Anolyte conductivity(k_{la})	5	$S \cdot m^{-1}$
Catholyte conductivity(k_{lc})	4.78	$S \cdot m^{-1}$
Current collector conductivity(k_s)	5000	$S \cdot m^{-1}$
Anolyte density(ρ_a)	1008.6	$Kg \cdot m^{-1}$
Catholyte density(ρ_c)	1004.9	$Kg \cdot m^{-1}$
Fuel initial concentration(c^0_{HCOOH})	0.5	$mol \cdot m^{-3}$
Oxygen initial concentration($c^0_{O_2}$)	1.25×10^{-3}	$mol \cdot m^{-3}$

where the electrons conduct to the cathode through an external circuit, meanwhile the protons diffuse to the oxidant flow across the interface between the liquid streams. At the cathode, the oxygen contained in the oxidant flow reacts with electrons taken from the electrode and protons from the sulfuric acid solution to form water. For all the operating and physical conditions involved in this model are listed in following Table 4.2.

4.5.3 Charge Balance

A Conductive Media DC application mode describes the potential distributions in the three subdomains using the following equations:

$$\begin{aligned} \nabla\cdot(k_s\nabla\phi_s) &= 0 \quad \text{in } \Omega_a \\ \nabla\cdot(k_l\nabla\phi_l) &= 0 \quad \text{in } \Omega_e \\ \nabla\cdot(k_s\nabla\phi_s) &= 0 \quad \text{in } \Omega_c \end{aligned} \tag{4.16}$$

Here k_s is the solid phase electronic conductivity (S/m) and k_l is the solution ionic conductivity (S/m). The potential (V) in the electrode phases is denoted by ϕ_s and that in the solution by ϕ_l. Electric insulation boundary conditions are applied to all the microchannel surfaces. Within the electrodes, we model the active layer of the two electrodes as boundaries, where charged species are generated or consumed, a current source is applied and the local current density is calculated by the Butler-Volmer equations.

For the electric potential, the electrode boundary conditions are identical, setting the boundary normal current density but using the opposite sign. In addition, the potential difference between the cathode and anode current collectors corresponds to the total cell voltage. Choose the potential at the anode current collector as the reference level by setting it to zero. Then the total cell voltage serves as the boundary condition at the cathode current collector:

$$\begin{aligned} \phi_s &= 0 \quad \text{at } \Omega_a, cc \\ \phi_s &= V_{cell} \quad \text{at } \Omega_c, cc \end{aligned} \tag{4.17}$$

As we discussed previously, the Bulter-Volmer charge transfer kinetics describes the charge transfer current density. At the anode, hydrogen is reduced to form water, and the following charge transfer kinetics equation thus applies:

$$i_{a,ct} = i_{0,a}[\frac{c_{Ox,a}}{c^0_{Ox,a}} exp(\frac{-\alpha_a nF}{RT}\eta_a) - \frac{c_{Red,a}}{c^0_{Red,a}} exp(\frac{(1-\alpha_c)nF}{RT}\eta_a)] \tag{4.18}$$

Here $i_{0,a}$ is the anode exchange current density (A/m^2), $c_{Ox,a}$ and $c_{Red,a}$ is the surface concentration of oxygen and fuel respectively (mol/m^3) around the anode, and $c^0_{Ox,a}$ and $c^0_{Red,a}$ is the bulk concentration of oxygen and fuel (mol/m^3) in the channels. Furthermore, F is Faraday's constant (C/mol), R the gas constant $(J/(mol \cdot K))$, T the temperature (K), and η_a the overpotential (V) on the anode.

For the cathode, the relation is used:

$$i_{c,ct} = i_{0,c}[\frac{c_{Ox,c}}{c^0_{Ox,c}} exp(\frac{-\alpha_a nF}{RT}\eta_c) - \frac{c_{Red,c}}{c^0_{Red,c}} exp(\frac{(1-\alpha_c)nF}{RT}\eta_c)] \tag{4.19}$$

Here $i_{0,c}$ is the cathode exchange current density (A/m^2), $c_{Ox,c}$ and $c_{Red,c}$ is the surface concentration (mol/m^3) of oxygen and fuel around the cathode respectively, and $c_{Ox,c}$ and $c_{Red,c}$ is the bulk concentration (mol/m^3) of oxygen and fuel around the cathode respectively.

In our microfluidic fuel cell model, since the overpotential on the anode is positive $(E_a > E_{r,a}, \eta_a > 0)$, which makes the first term of the Equation 4.18 negligible in comparison with the second term, that is, the oxidation current is predominant and the equation may be reduced to:

$$i_{a,ct} = -i_{0,a}\frac{c_{HCOOH,a}}{c^0_{HCOOH,a}} exp(\frac{(1-\alpha_c)nF}{RT}\eta_a) \tag{4.20}$$

Then it gives a negative current, which denotes that the electrons are leaving the electrode.

Similarly, the overpotential on the cathode is negative ($E_c < E_{r,c}, \eta_c < 0$), which makes the first term of the equation much larger then the second term, that is, the reduction current is predominant and the equation may be reduced to:

$$i_{c,ct} = i_{0,c}\frac{c_{O_2,c}}{c^0_{O_2,c}}exp(\frac{-\alpha_a nF}{RT}\eta_c) \tag{4.21}$$

These two Butler-Volmer equations are used for the boundary conditions of the reaction surface which are between the electrode and electrolyte for each side.

For the other boundaries we have electric insulation boundary conditions.

4.5.4 Hydrodynamic and Mass Transport

According to the specifications, the flow rate at the inlet is roughly 0.08 mm/s. This implies a low Reynolds number as 1.6×10^{-4} for the sulfuric acid supporting electrolyte solution in the microchannel:

$$Re = \frac{\rho du}{\eta} = \frac{10^3 \times 2 \times 10^{-9} \times 8 \times 10^{-5}}{10^{-6}} = 1.6 \times 10^{-4} \tag{4.22}$$

Thus it is easy to get a numerical solution of the full momentum balance and continuity equations for incompressible flow with a reasonable number of elements. The equations that we have solved are the Navier-Stokes equations at steady state:

$$\begin{aligned} \Delta u &= 0 \\ 0 &= -\frac{1}{\rho}\nabla p\vec{i} + \nabla^2 \cdot (\mu \vec{ui}) \end{aligned} \tag{4.23}$$

Here ρ denotes density (kg/m^3), u is the velocity (m/s), μ denotes viscosity (Pa).

In the microchannel domain, it has those electrolyte flow, our model uses Convection and Diffusion application mode.

$$-\nabla\cdot(-D\nabla c + cu) = 0 \tag{4.24}$$

In this equation, D denotes the diffusion coefficient (m^2/s) and c represents the concentration (mol/m^3).

At the inlets and outlets of the microchannel, pressure condition apply along with vanishing viscous stress:

$$\begin{aligned} p &= p_0 \\ n\cdot\mu\nabla u &= 0 \end{aligned} \tag{4.25}$$

Setting the pressure at the outlets to atomspheric pressure, the pressure at the inlets represents the pressure drop over the cell.

At the walls, *No – slip* conditions state that the velocity is zero:

$$(u, v) = (0, 0) \quad \text{at the walls} \tag{4.26}$$

For the mass balances, at the inlets, the concentration is used boundary condition with the following values:

$$\begin{aligned} &c_{HCOOH} = c_{0,HCOOH} \quad \text{at the anode inlet} \\ &c_{O_2} = 0 \quad \text{at the anode inlet} \\ &c_{HCOOH} = 0 \quad \text{at the cathode inlet} \\ &c_{O_2} = c_{0,O_2} \quad \text{at the cathode inlet} \end{aligned} \tag{4.27}$$

For the concentrations of rest species which are sulfuric ions and hydrogen ions, we assume that they are large enough to be uniformly constant values throughout the microchannel.

At the outlet, convective flux dominates mass transport and the concentration gradient normal to the outlet is set to zero.

$$(-D\nabla c_i)\cdot n = 0 \quad \text{at the outlets} \tag{4.28}$$

where c_i is the concentration for species i.

On the channel walls, which are the places where electrochemical reactions occurred, we set the boundary condition as mass fluxes generated by the reactions based on Butler-Volmer equations, mentioned above:

$$-n\cdot N_{HCOOH}|_{anode} = \frac{i_{a,ct}}{F} \tag{4.29}$$

$$-n\cdot N_{O_2}|_{cathode} = \frac{2i_{c,ct}}{F} \tag{4.30}$$

4.5.5 Results

For the 2-Dimensional steady-state simulations, all time-derivatives in the governing equations are set to zero, the boundary conditions mentioned above are applied. A stationary linear solver and a direct solver using Unsymmetric MultiFrontal method with UMFPACK. Since the Bulter-Volmer reaction kinetics expression creates bidirectional coupling between the potential and convection-diffusion equations, the two modules must be solved simultaneously in order to obtain an accurate solution.

Meshing the model using finner mesh size, it converges within 2.438 seconds using a triangular mesh of 3794 elements with 43962 degrees of freedom. The model was solved on a 62-bit Windows 7 platform, with an intel core i7 2.8 GHz quad-core processor. Peak memory usage was observed to be about 6 GB. Run-times to complete a polarization curve with 9 points were about 5 minutes.

As mentioned above, for the 2-Dimensional model, it only focuses on how to achieve the complete model, so the following results only show one sets of working condition without comparison from some others.

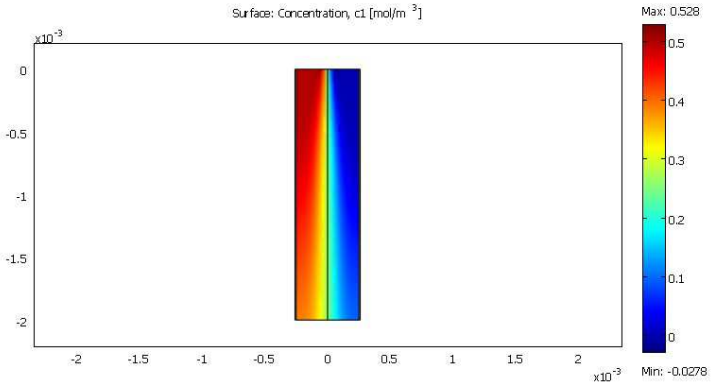

Figure 4.7: HCOOH concentration distribution in 2D model

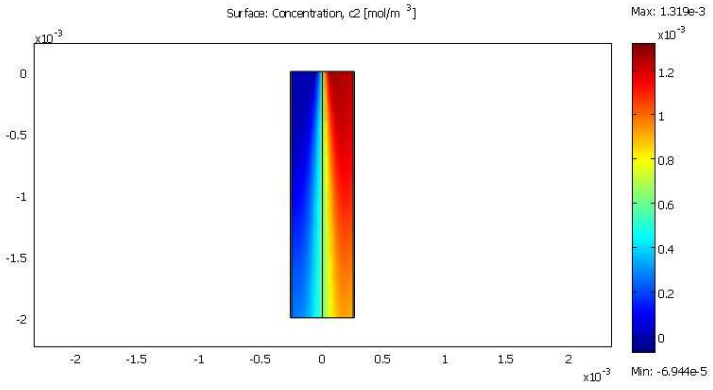

Figure 4.8: Oxygen concentration distribution in 2D model

The Figure 4.7 and 4.8 above give a clear illustration of the concentration profiles in the channel domain, showing slow mixing by interdiffusion of the two

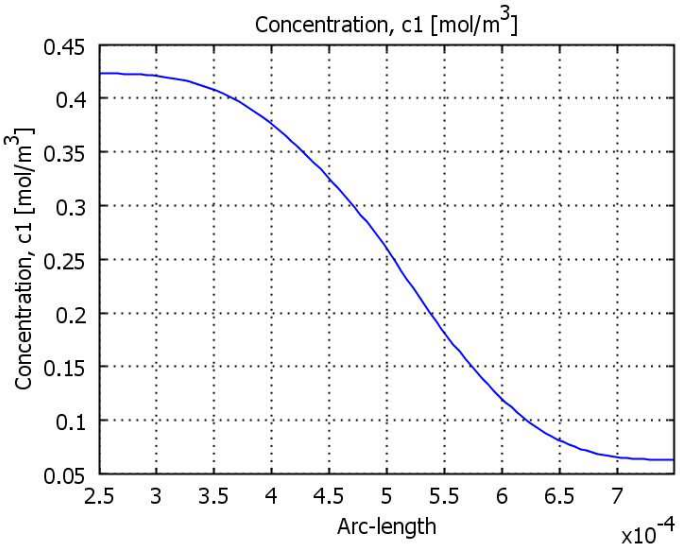

Figure 4.9: HCOOH concentration distribution of the cross section on 10mm from the outlets

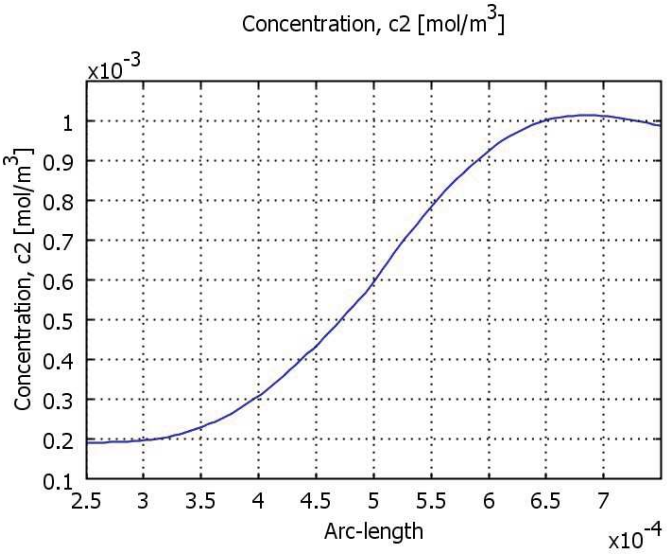

Figure 4.10: Oxygen concentration distribution of the cross section on 10mm from the outlets

streams at the liquid-liquid interface, and to be more specific, in Figure 4.9 and 4.10, the concentration distribution of HCOOH and Oxygen at the cross-section 10mm from the outlets of the channel are presented. By looking carefully at the electrodes which are showing on two sides of the plots, it can be found that the peak values of the concentration are not located at the surface of electrodes but around,

which indicates that there are fluxes occurring on the electrode surfaces consuming the concentration of species by electrochemical reactions. However, comparing to the decrescent of concentration in the inter-diffusion zone, the diffusive flux on the electrode surface is much less then the diffusive exchange in the middle of channel.

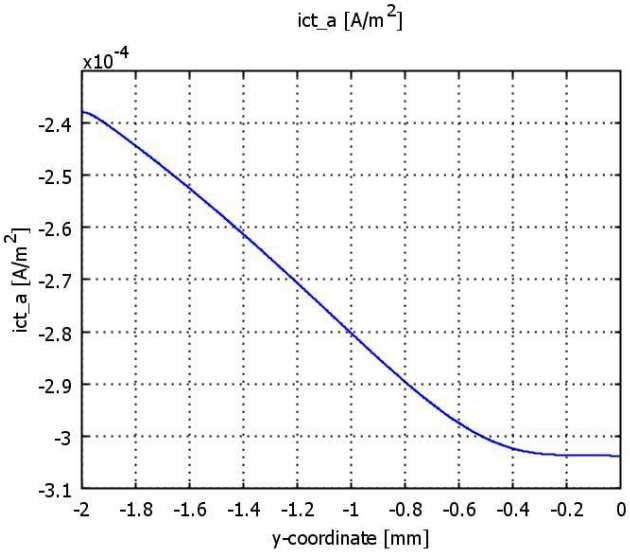

Figure 4.11: Current density along the anode

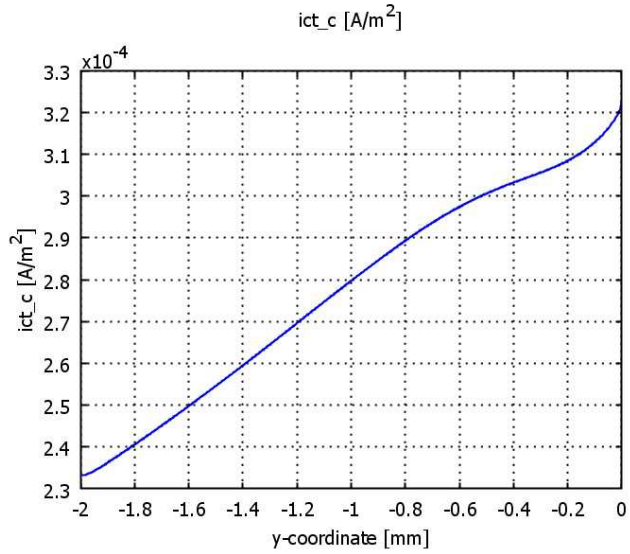

Figure 4.12: Current density along the cathode

The current density distribution along the anode and cathode are given in Figure 4.11 and 4.12 above, respectively. The current density is uneven with the highest density in the cell's upper region, where starting from 0 on x-axis. This means that the electrochemical reaction rate in the electrodes determines the current-density distribution, since the species concentration is decreasing along the channel sides from the inlets. The maximum current density arises close to the channel inlets. Additionally, by comparing these two approximately inverse curves, it is easy to see that they have the same amount but opposite value, since the model has a closed circuit.

To conclude, in this two dimensional modeling work, it provided a complete understanding corresponding main principles of microfluidic fuel cell in COMSOL Multiphysics ®, which includes incompressible Navier-Stokes module, convection and diffusion module, and two conductive media DC modules for electrodes and electrolyte. After this, by coupled these for modules in one model, it is able to calculate the channel length on the premise of avoiding the inter-diffusion zone reach the electrode reaction diffusion layer. Besides, this work also provided a validate modeling way to obtain set of necessary results regarding to the analysis of cell performance in the coming three dimensional modeling work.

4.6 3-Dimensional Model

4.6.1 Model Introduction

In this section, an integrate numerical 3-Dimensional model of microfluidic fuel cell has been built by COMSOL® based on the 2-Dimensional model, and the porous catalyst layer is also introduced in this model, since that we adopt the Solid Oxide Fuel Cell model from COMSOL®'s model library, which contains two catalyst layers

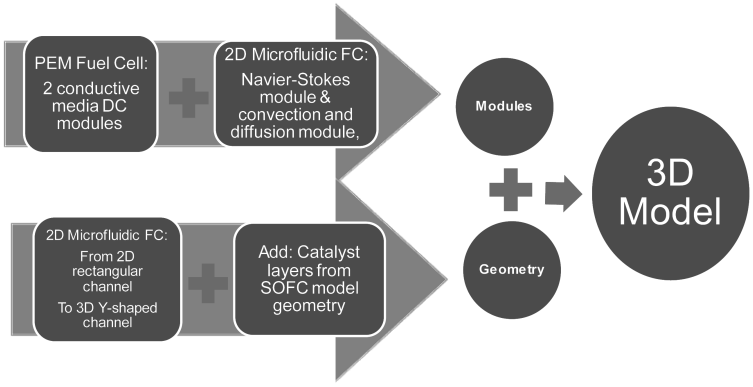

Figure 4.13: Procedure of building final 3D microfluidic fuel cell model

configuration. For the coupled modules, this multiphysics work contains as well incompressible Navier-Stokes module, convection and diffusion module, and two conductive media DC module for electrodes and electrolyte. These four modules help to form a complete fuel cell model. This model simulates the electrochemical reaction on each electrode with the Butler-Volmer equations which assisting the module to couple with convection and diffusion module, additionally, it simulates the flow mechanics by using Navier-Stokes equation. Different from 2-Dimensional model, this work is using all specific settings for working condition from the experimental work done by Falin Chen et al.(*30*); the model has been developed to determine the effect of the channel geometry and feature of catalyst layer on cell performance basing on polarization curves and power density curves. The Figure 4.13 shows the whole procedure of building this three dimensional microfluidic fuel cell model.

4.6.2 Model Definition

As we can see, on Figure 4.14, and the cross section of the fuel cell channel on Figure 4.15 consists of six domains: an anode (Ω_a) as $C01$, a cathode (Ω_c) as $C03$, two electrolyte flow domain (Ω_{ea}) as $C05$, (Ω_{ec}) as $C02$, and two catalyst layer (Ω_{ca}) as $C06$, (Ω_{cc}) as $C04$. Two current collectors are located on the front surface of

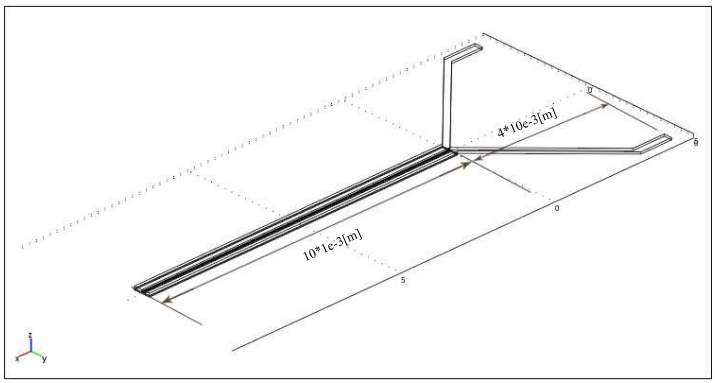

Figure 4.14: 3D Model geometry

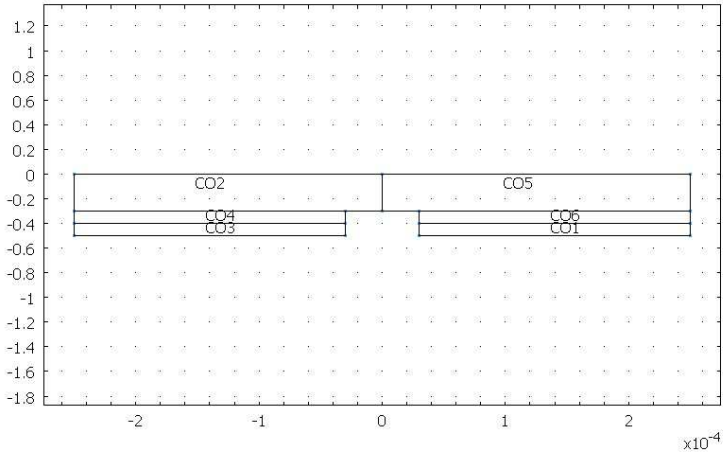

Figure 4.15: 3D Model cross section profile

each electrode. The microchannel has two inlets and two outlets, which are located on the top and bottom respectively, since this cell geometry is symmetrical, it has been divided into half as shown in Figure 4.16, the red parts are the channels. The design aims to avoid upsets in the flow field when the two streams are united. This is to avoid the two streams mixing through convection, which would mix all species equally and lead to loss of control over the separation abilities. The transport of

species between streams should take place only by diffusion in order that species with low diffusion coefficients stay in their respective streams.

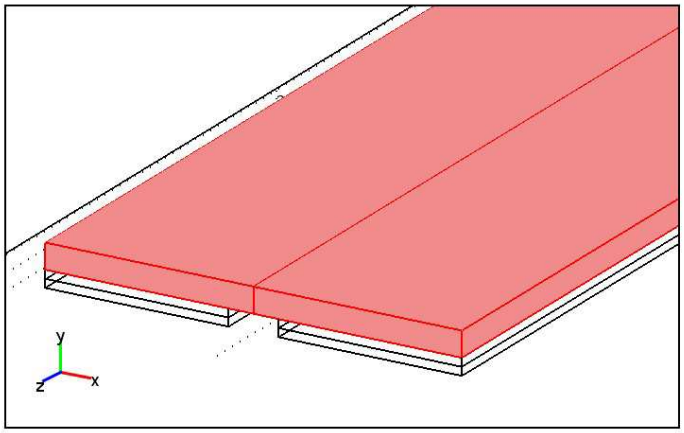

Figure 4.16: 3D Model outlets part view

This model treats quadrangular prism with two channels for separation through diffusion. The cell puts two different laminar streams in contact for a controlled period of time. The contact surface is well defined, and by controlling the flow rate it is possible to control the amount of species transported from one stream to the other through diffusion.

The geometry of the channels takes the size length and width of the 2-Dimensional model's, with $125\mu m$ as half height which gives a relatively high aspect ratio of channel cross section. This design is based on the study of Bazylak et al. (*7*), which concluded that the rectangular geometry with a high aspect ratio in the cross-stream direction provides better cell performance and fuel utilization compared with other designs. For those two electrodes, they have the same length as channels, and $50\mu m$ as height, with the results of 2-Dimensional modeling, we set the width as $220\mu m$, which left a $60\mu m$ gap as diffusion width at the outlets of the channel between those two electrodes. As showed in Figure 4.14.

Table 4.3: Operating and physical conditions for 3-Dimensional microfluidic fuel cell

Parameter	Value	Unit
Faraday's constant(F)	96500	$C \cdot mol^{-1}$
Atmospheric pressure(P_{atm})	1	atm
Overpressure, anode inlet(ΔP_a)	0.25	Pa
Overpressure, cathode inlet(ΔP_c)	0.5	Pa
Temperature(T)	25	°C
Gas constant(R)	8.314	$J \cdot mol^{-1} \cdot K^{-1}$
Viscosity of all solutions(μ)	0.001	$Kg \cdot m^{-1} \cdot s^{-1}$
Diffusivity of catholyte(D_c)	2.1×10^{-9}	$m^2 \cdot s^{-1}$
Diffusivity of anolyte(D_a)	2.546×10^{-9}	$m^2 \cdot s^{-1}$
Anodic exchange current(i_{0a})	3.82×10^5	$A \cdot m^{-2}$
Cathodic exchange current(i_{0c})	100	$A \cdot m^{-2}$
Anode specific surface area(S_a)	10^5	m^{-1}
Cathode specific surface area(S_c)	10^5	m^{-1}
Initial cell polarization(V_{pol})	0.05	V
Anodic equilibrium voltage($\Delta\phi_{eqa}$)	0.2	V
Cathodic equilibrium voltage($\Delta\phi_{eqc}$)	1.23	V
Anolyte conductivity(k_{la})	11.47	$S \cdot m^{-1}$
Catholyte conductivity(k_{lc})	43	$S \cdot m^{-1}$
Current collector conductivity(k_s)	10^7	$S \cdot m^{-1}$
Anolyte density(ρ_a)	1008.6	$Kg \cdot m^{-1}$
Catholyte density(ρ_c)	1004.9	$Kg \cdot m^{-1}$
Fuel initial concentration(C^0_{HCOOH})	0.5	$mol \cdot m^{-3}$
Oxygen initial concentration($C^0_{O_2}$)	1.25×10^{-3}	$mol \cdot m^{-3}$
Molar mass of HCOOH(M_{HCOOH})	46	$g/moll$
Molar mass of O_2(M_{O_2})	32	$g/moll$

The same electrochemical reactions take place in this model, with operating and physical conditions in Table 4.3 above.

4.6.3 Charge Balance

Similarly, 3-Dimensional model adopted two Conductive Media DC application modes to describe the potential distributions in the six subdomains using the Equations 4.31.

As we see in Equations 4.31, κ_{lc} and κ_{la} are the catholyte and anolyte phase electronic conductivity (S/m). The potentials (V) in these two phases are denoted by ϕ_{lc} and ϕ_{la}. ϕ_c is the potentials (V) of the catalyst layers, and $S_a i_{ct}$ denotes the specific surface area S_a $(1/m)$ times the charge transfer current reaction density i_{ct} (A/m^2). For the remaining parameters, they have the same meaning as mentioned before. Electric insulation boundary conditions are applied to all the microchannel surfaces. Within the electrodes, we model the active layer of the two electrodes as boundaries, where charged species are generated or consumed, a current source is applied and the local current density is calculated by the Butler-Volmer equations.

$$\begin{aligned}
\nabla\cdot(\kappa_s\nabla\phi_s) &= 0 \quad \text{in } \Omega_a \\
\nabla\cdot(\kappa_s\nabla\phi_s) &= 0 \quad \text{in } \Omega_c \\
\nabla\cdot(\kappa_{lc}\nabla\phi_{lc}) &= 0 \quad \text{in } \Omega_{ec} \\
\nabla\cdot(\kappa_{la}\nabla\phi_{la}) &= 0 \quad \text{in } \Omega_{ea} \\
\nabla\cdot(\kappa_s\nabla\phi_c) &= S_a i_{ct} \quad \text{in } \Omega_a \\
\nabla\cdot(\kappa_s\nabla\phi_c) &= S_a i_{ct} \quad \text{in } \Omega_c
\end{aligned} \tag{4.31}$$

For the electrical potential boundary, and we applied the same setting as in 2-Dimensional model.

4.6.4 Hydrodynamic and Mass Transport

Similarly, we applied the same boundary settings for Navier-Stokes module in our 3-Dimensional model.

For the convection and diffusion equation module, it is applied in all the domains including two microchannel domains and two electrode domains, for the reason that we consider catalyst layer on the surface of the electrode where reactant species are consumed with a given rate.

At the anode, dilute sulfuric acid with formic acid flow as fuel. An the cathode, oxidant dissolved in dilute sulfuric acid is supplied.

The material transport is described by convection and diffusion equations. In the stationary case, the mass balance is governed by:

$$\nabla\cdot(-D\nabla c_i) = R - \overrightarrow{u}\cdot\nabla c_i \tag{4.32}$$

Here D denotes the diffusion coefficient(m^2/s), c_i represents the concentration (mol/m^3) of specie i, $\overrightarrow{u}$ is the velocity vector, and R is the species consuming rate $mol/(m^3\cdot s)$.

In the open channels, set the reaction source term to zero. However, in the catalysts layer which here is electrode domain, the source term is given by the electrochemical reaction rate. It is calculated from the charge transfer current density according to Faraday's law:

$$R_i = v_i\frac{i_{ct,i}}{n_i F} \tag{4.33}$$

where v_i is the stoichiometric coefficient and n_i is the number of electrons in the reaction. $i_{ct,i}$ is the current density.

For the boundaries, at the inlets, the concentration boundary condition is used with the following values:

$$
\begin{aligned}
&c_{HCOOH} = c_{0,HCOOH} \quad \text{at the anode inlet} \\
&c_{O_2} = 0 \quad \text{at the anode inlet} \\
&c_{HCOOH} = 0 \quad \text{at the cathode inlet} \\
&c_{O_2} = c_{0,O_2} \quad \text{at the cathode inlet}
\end{aligned}
\tag{4.34}
$$

For the concentrations of rest species which are sulfuric ions and hydrogen ions, we assume that they are large enough to be uniformly constant values throughout the microchannel.

At the outlet, convective flux dominates mass transport and the concentration gradient normal to the outlet is set to zero:

$$
(-D\nabla c_i)\cdot n = 0 \quad \text{at the outlets} \tag{4.35}
$$

where c_i is the concentration for species i.

On the channel walls, which are the places where electrochemical reactions occurred, we sett the boundary condition as the mass fluxes generated by the reactions based on Butler-Volmer equations, are determined by the electrochemical reaction rate:

$$
-n\cdot N_{HCOOH}|_{anode} = \frac{i_{a,ct}}{F} \tag{4.36}
$$

$$
-n\cdot N_{O_2}|_{cathode} = \frac{2i_{c,ct}}{F} \tag{4.37}
$$

4.6.5 Mesh and Validation

Mesh optimization plays a significant role in solving CFD problem. In this work, the mesh type used is a non-uniform, triangular mesh. As a means of validation, the global and local mesh sizes were increased until further refinements yielded no

Table 4.4: Different MESHs and corresponding NOFS, NE, and SOLUTION TIME

MESH	NOF	NE	SOLUTION TIME(s)
Extra coarse	30319	2897	271.006
Coarser	52949	5378	1078.426
Normal	120231	13026	2105.25
Fine	175965	20287	4626.234

any appreciable changes in the results. At the Table 4.4 the different meshes and corresponding parameters such as the Number of Degrees of Freedom (NOF), the Number of Elements (NE) and the solution time as well.

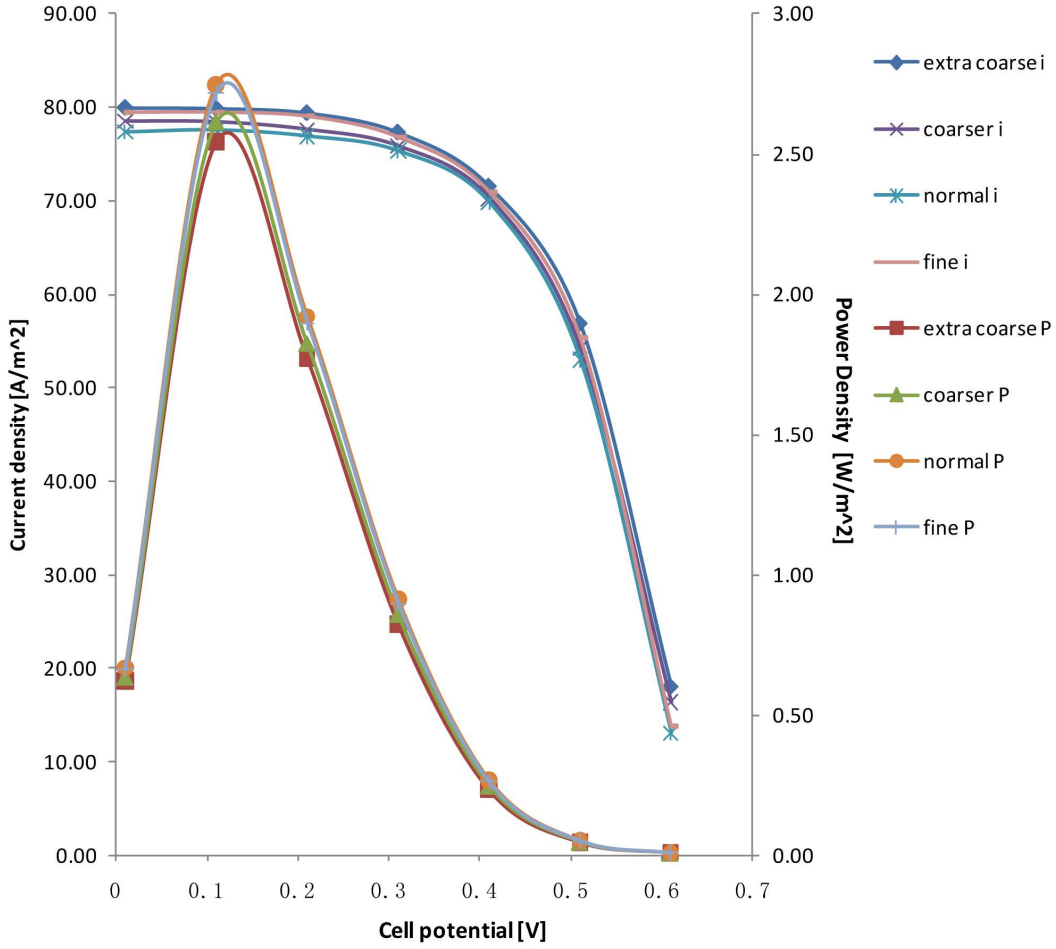

Figure 4.17: Solution convergence from different meshes

The Figure 4.17 shows the tendency of cell performance changing by different meshes. By looking carefully, it is clear that there is no appreciable changes when the mesh reaches fine mesh from normal mesh, which indicates that it is not necessary to do any further meshes rather than normal mesh, to be more specific, the cell performance reaches the highest when the normal mesh applies.

In order to validate this Y-shaped design, the comparison with the model reported by Chang et al. (*3*). The conditions applied in that experimental work is applied in this modeling work. The electrolyte is flowing at $0.5ml/min$ using $2.1M$ formic acid as the fuel and oxygen saturated $0.5M$ sulfuric acid as oxidant. The results of the developed model compared to those reported by Chang et al. (*3*) are shown in Figure 4.18, and the current and power were conventionally normalized by the electrode surface area. It is clear that the results are in good agreement.

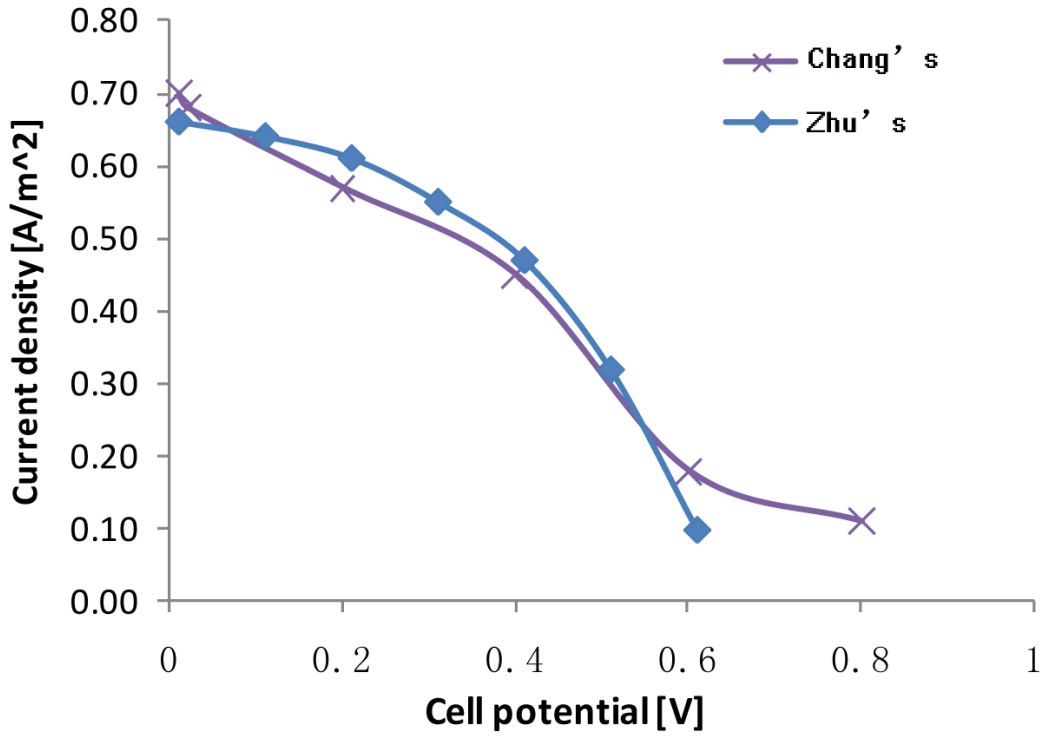

Figure 4.18: Verification of the proposed model against the results reported by Chang et al. (*3*) for a numerical model results

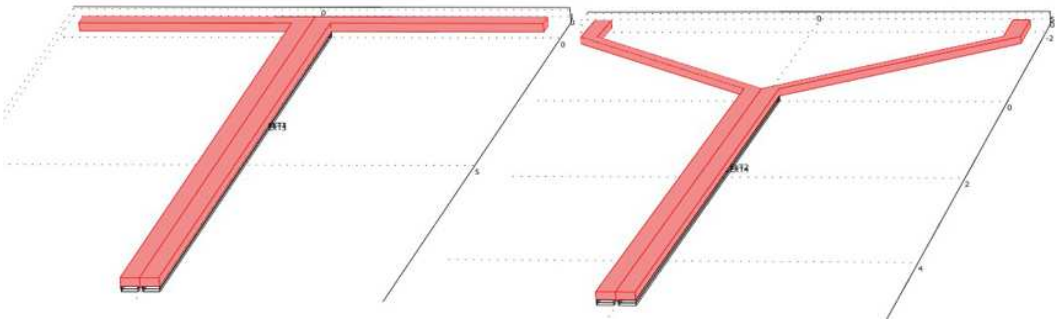

Figure 4.19: T- and Y-shaped microchannel designs

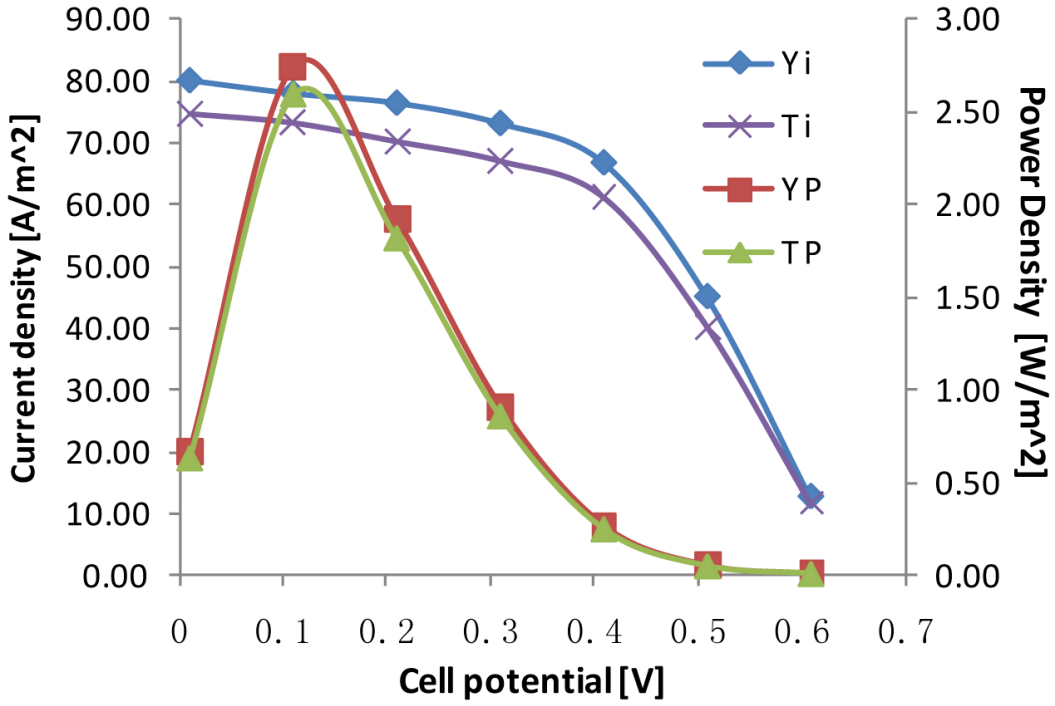

Figure 4.20: Comparison of cell performance between Y- and T-shaped channel design

Generally, the microfluidic fuel cell has the T- or Y-shaped designs for microchannel. Bazylak et al.(*7*) has presented a numerical work on T-shaped design, and Chang et al.(*3*) has presented a numerical work on Y-shaped design, however, there's no comparison has been done. Since that, in this work both Y- and T-shaped design have been built as shown in Figure 4.19. For these two model, we applied the same design on for both configuration except the convergence design, so they

both have same electrode length and channel cross section which make them have the same electrochemical kinetic.

Figure 4.20 gives the view of these two designs current densities and cell performances. From this comparison, it is clear that Y-shaped microchannel design makes higher current density and better cell performance, which can be explained that Y-shaped convergence angle makes better division between the fuel and oxidant.

4.6.6 Results

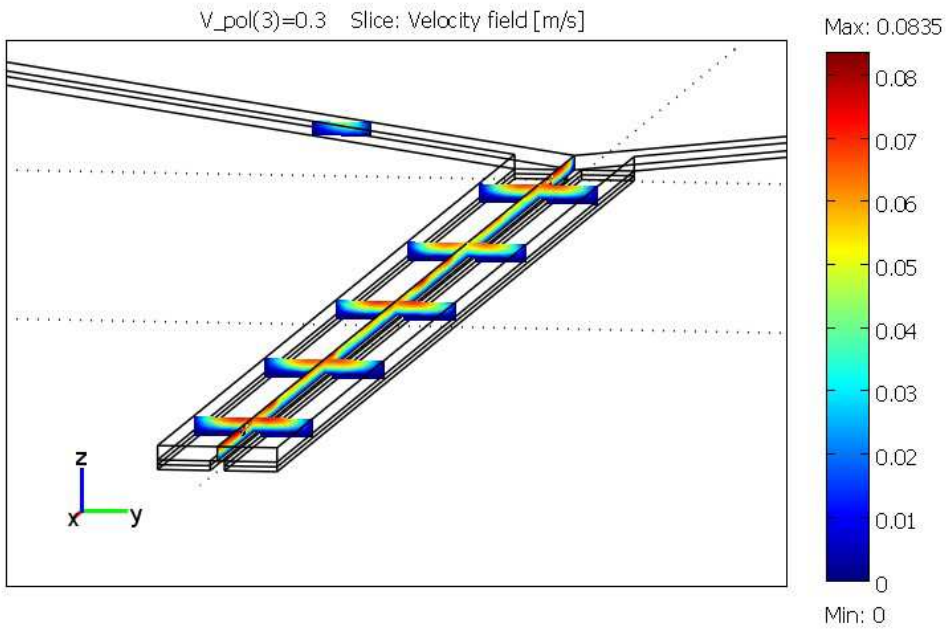

Figure 4.21: 3D Model velocity profile

For the 3-Dimensional steady-state simulations, all time-derivatives in the governing equations are set to zero, the boundary conditions mentioned above are applied. A parametric sweep was adopted to calculate the current density at different cell voltages. The stationary linear solver was chosen as Unsymmetric Multi-

Frontal method with UMFPACK. Since the Bulter-Volmer equation is applied to create bidirectional coupling between the AC/DC module and convection and diffusion equation module, the two have to be solved simultaneously in order to obtain an accurate solution. However, the coupling of these equations results in a set of non-linear equations for which it is difficult to obtain convergence from the COMSOL®'s non-linear solver. Therefore, instead of solving the modules in a coupled manner, it is recommended to solve this system of equations in an iterative manner. In this study, these four modules have been divided in two groups such as convection and diffusion equation module boned with incompressible Navier-Stokes equation module, and two AC/DC modules boned together. The first group is solved firstly, and then base on the solution it obtained, the second group is solved consistently.

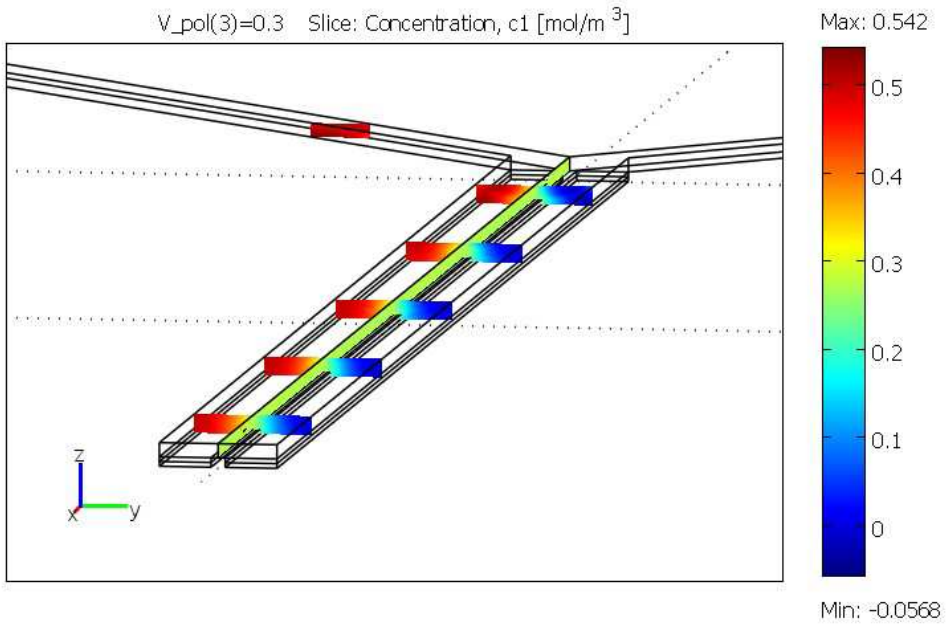

Figure 4.22: 3D Model *HCOOH* concentration distribution

In this modeling work, there are several governing partial differential equations (PDEs) which are describing in the physics of this microfluidic fuel cell operation,

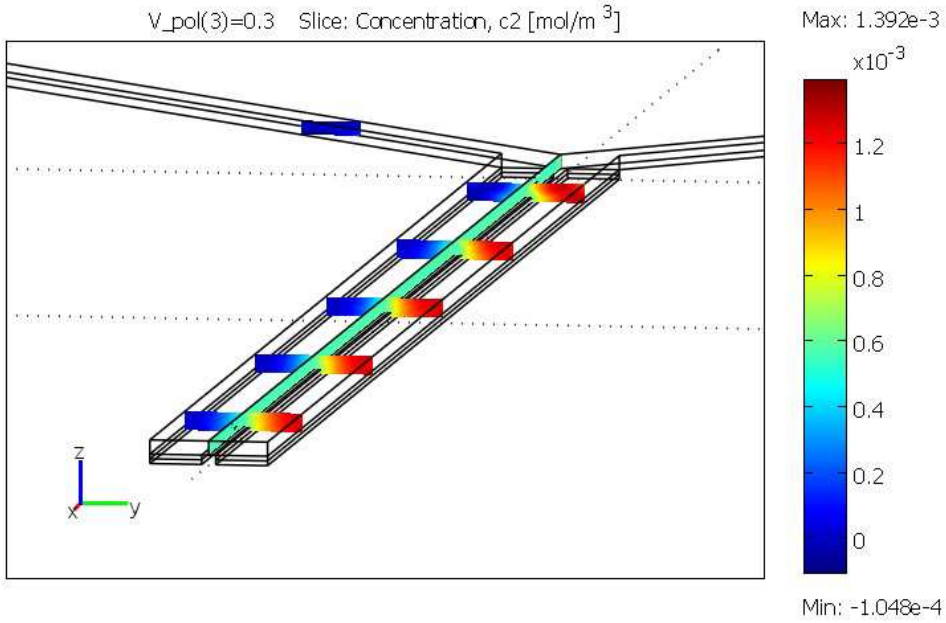

Figure 4.23: 3D Model O_2 concentration distribution

such as Navier-Stokes equations, diffusion and convection equations, and equations corresponded with charge balances. They are all solved by COMSOL® using finite element (FEM) numerical techniques for the spatial discretization. To be more specific, the stabilized finite element methods are formed by adding to the standard Galerkin method variational terms that are mesh-dependent, consistent and numerically stabilizing (*31*).

Meshing the model was performed using normal mesh size, using a triangular mesh of 13026 elements with 120231 degrees of freedom. The model was solved on a 62-bit Windows 7 platform, with an intel core i7 2.8 GHz quad-core processor. Peak memory usage was observed to be about 6 GB. Run-times to complete a polarization curve with 7 points were about 45 minutes.

Figure 4.21 shows the velocity profiles of reactants in the microchannel with P_{in} as 20 Pa. Figure 4.22 and 4.23 show the distribution of $HCOOH$'s and O_2's concentration respectively.

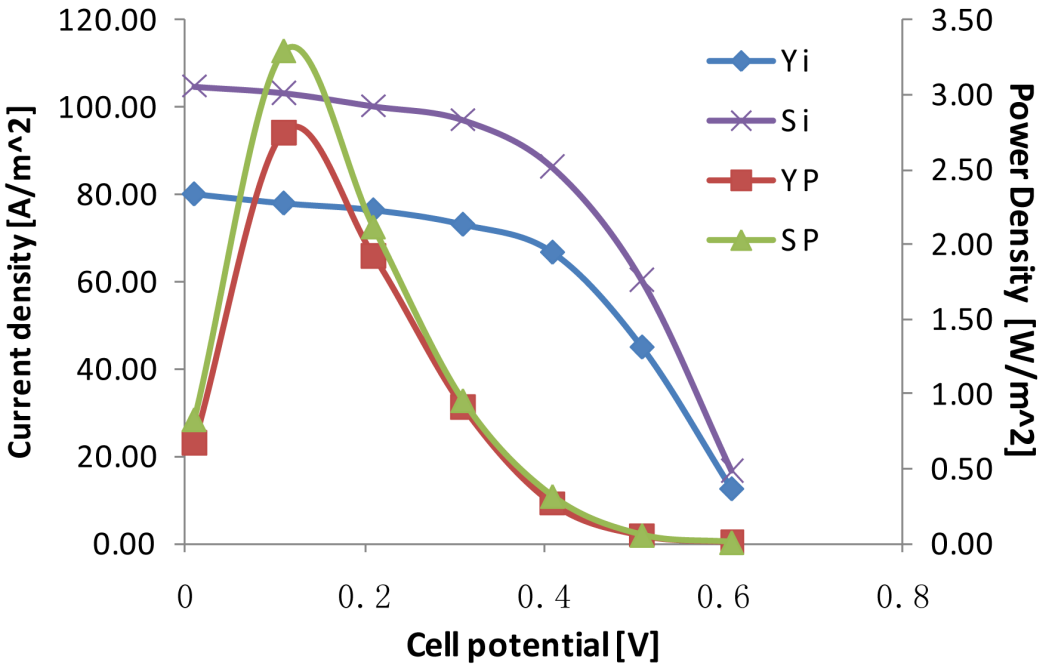

Figure 4.24: The current and power density curves for three assigned inlet pressure.

Since the modeling work setting is using the working condition from the experimental work of Choban et al.(*4*)'s, so we firstly presented the comparison of these two works. Both cases are considered to work in the same condition, by using the parameters' list in Table 4.3 and under the same flow rate condition. The results are illustrated in Figure 4.25 where contains Y-shaped microchannel design and straight microchannel design as in the experimental work. This straight microchannel design is just a design for comparison which gives the ideally best cell performance that modeling work is hardly able to achieve. It clearly shows that Straight design has better cell performance than the Y-shaped channel design, and for the straight channel design, both numerical and experimental work have been done and it shows that numerical work has higher cell performance than the exper-

imental work. Accordingly, the present results could provide not only qualitatively but also quantitatively theoretical predictions. In the following paragraphs, we will take the condition mostly based on the list in Table 4.3 with some modifications. The effects of some parameters including convergence angle, flow rate, concentration, and catalyst layer, on the transport characteristics of reactants in both anode and cathode streams as well as the cell performance will be described in detail based on this condition.

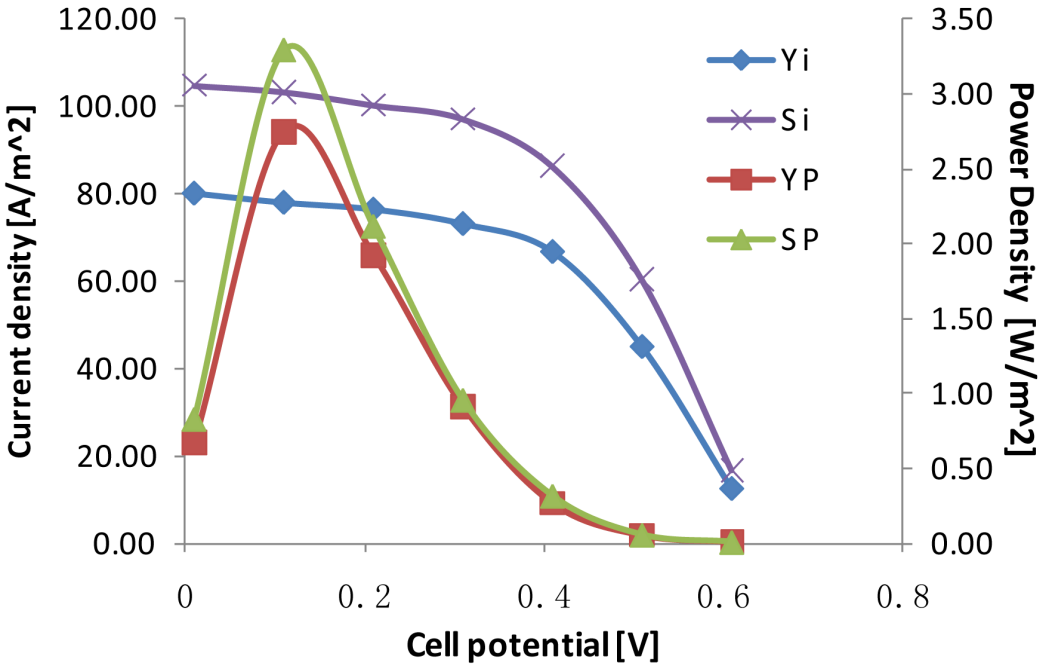

Figure 4.25: The current and power density curves for three assigned inlet pressure.

Effects of convergence angle of Y-shaped channel

As mentioned, this study is based on the experimental work done by Falin Chen et al.(*30*), using Y-shaped microchannels to separate anode and cathode liquid streams at different inlets and then flow in parallel through the microchannel without occurrence of turbulent mixing on the contact interface of both streams. The convergence angle of the Y-shaped inlets is an factor effecting the flow in the channel. In this

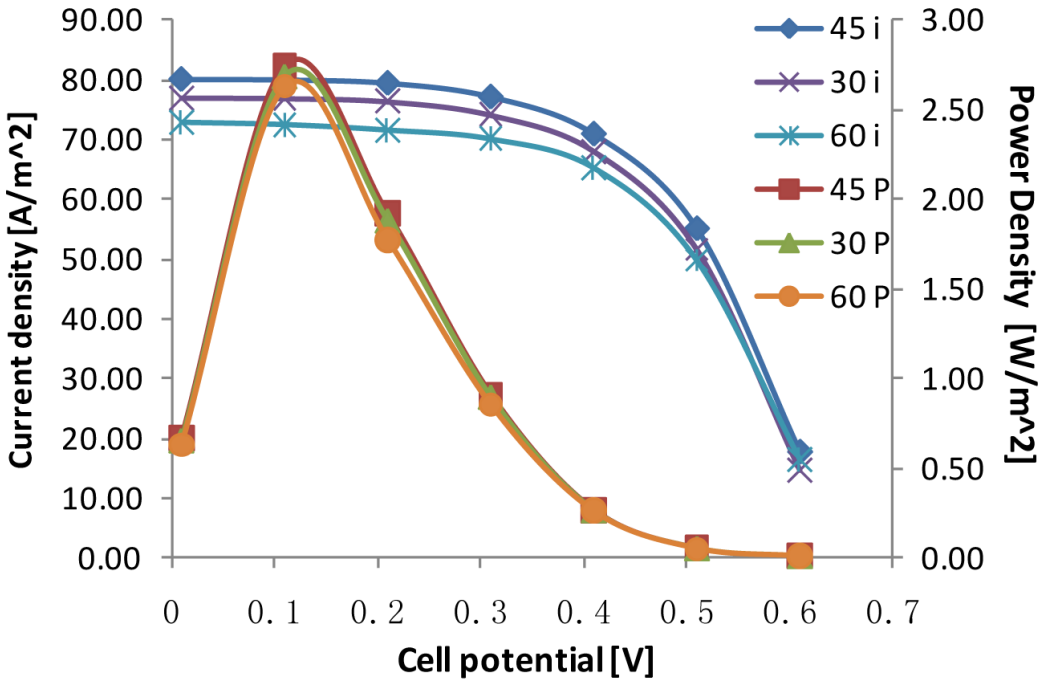

Figure 4.26: The current and power density curves for three assigned convergence angle.

study, three angles have been choose to study the cell performance. The corresponding $I-V$ and power density curves are demonstrated in Figure 4.26. Looking carefully, the best cell performance and power density is for the angle of 45°. Therefore, the convergence angle is not a significant factor which mainly effects the cell performance, since the differences between these three convergence angles design are not big.

Effects of volumetric flow rate

The volumetric flow rate, Q, is an significant factor for the performance of laminar flow-based microfuel cell, where Q is the combination of equal flow rates of the fuel and oxidant streams in the microchannel. If Q is too low, both fuel and oxidant streams will have more time to be in diffusional contact and thus cause a higher degree of mixing. In this study, Q is defined by giving inlet pressure P_{in}, which is the pressure drop from atmosphere pressure. The corresponding $I-V$ and power

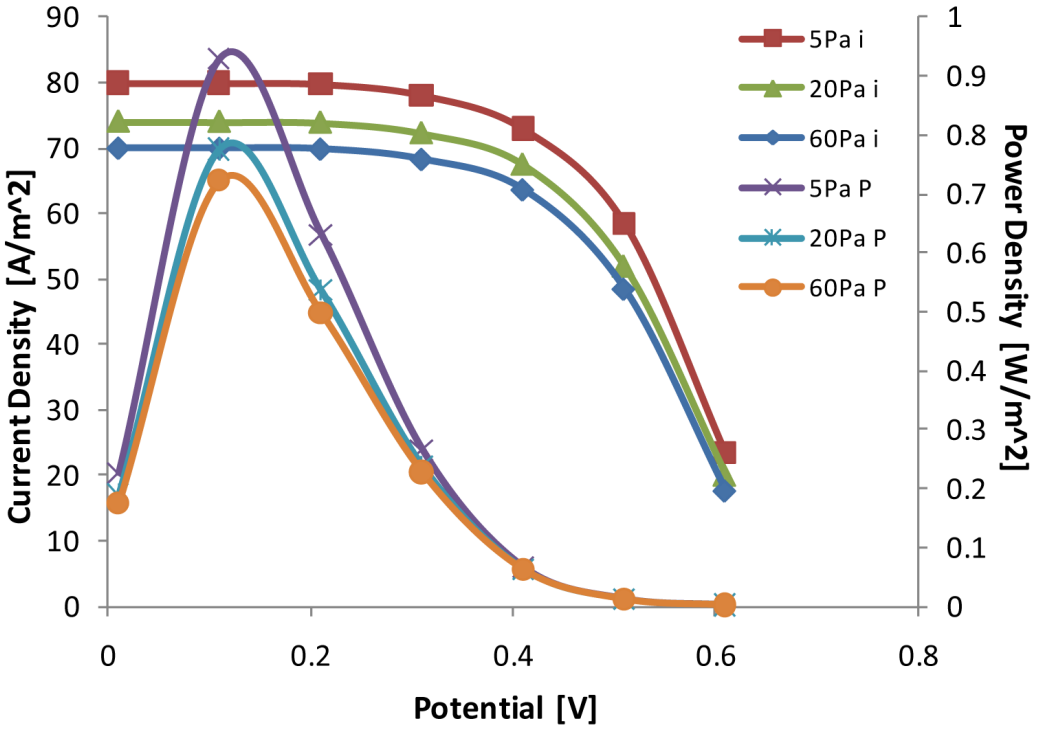

Figure 4.27: The current and power density curves for three assigned inlet pressure.

density curves are given in Figure 4.27. Clearly, it has the higher current density and power density which represent the cell performance in the low cell potential region when supplying lower pressure drop.

These results indicate that it has to choose pressure from low pressure drop, however, if the flow rate becomes to too low, which leads to the increasing of diffusion of reactants which were supposed to react on the surface of electrodes, it will decrease the cell performance from lowering the reaction rate. Therefore, we have to keep the flow rate in a relative low scale in order to both have high reaction rate and enough time for complete reaction on the electrode surface.

Effects of concentrations of reactants

To examine the effects of concentration on cell performance, we first consider the concentration of formic acid in anode stream. It is expected that its influence should

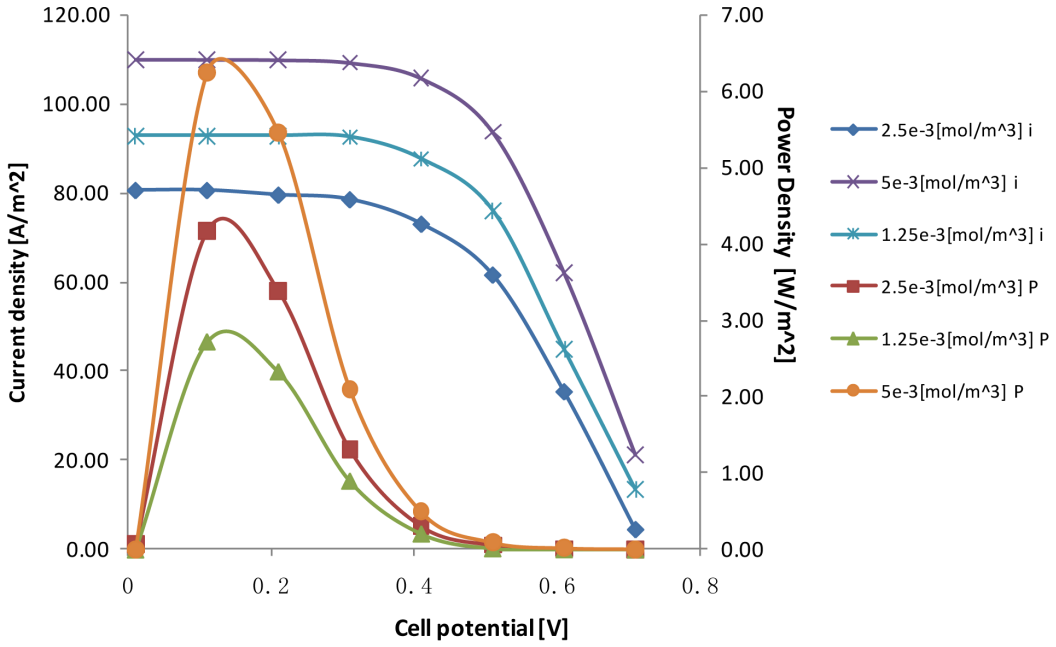

Figure 4.28: The current and power density curves for three assigned concentrations of oxygen.

be small since the cell performance is primarily cathode-limited (*4*). The cell performance is sensitive to the variation of oxygen concentration in cathode stream, as we can see in Figure 4.28 which illustrates the $I-V$ curves for these assigned values of oxygen concentration. Obviously, the cell performance can be improved significantly by increasing the oxygen concentration, which could be done by dissolving more oxygen into oxygen solution stream.

Effects of catalyst layers' porosities

For the reason that the cell performance is significantly limited by cathode, we moved our attention to the effects of cathode catalyst layer. Assuming that these layers are made by the deposition of platinum particles uniformly on the thin porous substrates, with three assigned porosities. The $I-V$ and power density curves are demonstrated in Figure 4.29. One can see that the cell reached the highest performance when the porosity is 0.4, for the other values of porosity, the performance

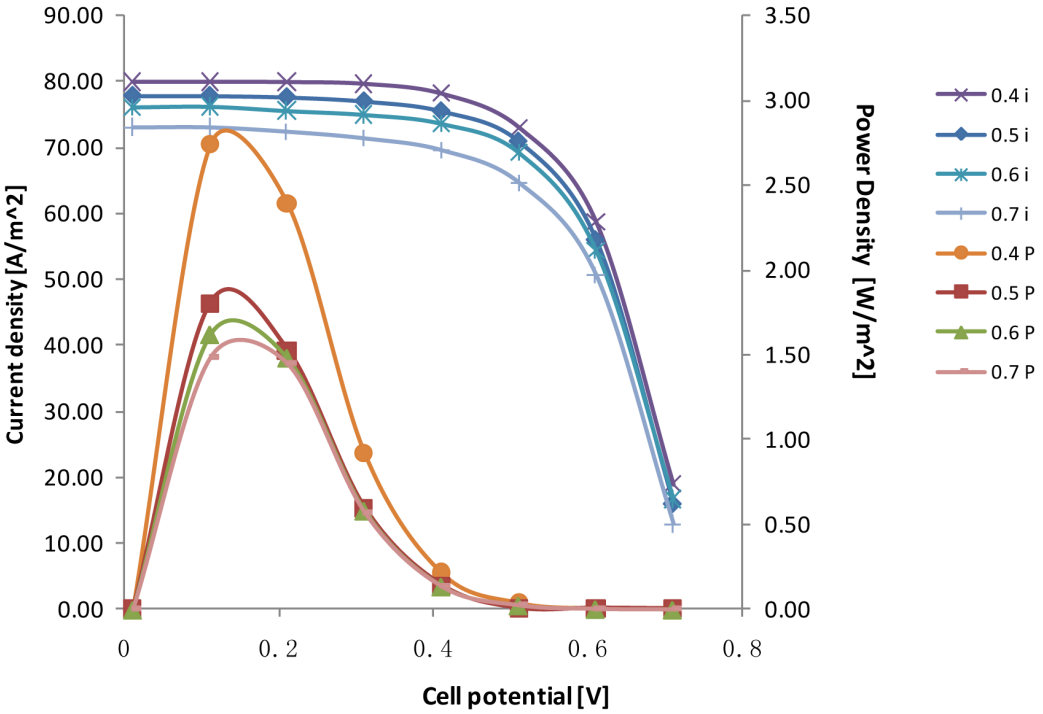

Figure 4.29: The current and power density curves for three assigned porosities of cathode catalyst layer.

are all similar. It is also noted that the porosity of the anode catalyst layer plays a minor role only on the cell performance.

Summary Overview

To sum up, in this modeling study of microfludic fuel cell, the convergence angle of the microchannel, pressure drop between inlets and outlets of the microchannel, concentration of oxidant solution, and porosity of catalyst layer have been investigated. The results show that with 45°convergence angle, the cell has the best performance; when the cell is applied on 60 *Pa* pressure drop between the inlets and outlets, it shows better performance rather than 20 *Pa* and 100 *Pa*; the higher concentration of oxidant, the better cell performance it can achieve; additionally, it shows the best cell performance when the porosity of catalyst layer is 0.4.

Chapter 5

CONCLUSIONS AND FUTURE DIRECTIONS

In this dissertation, the background and motivation for microfluidic fuel cells were presented in chapter 1, as well as the particular objectives; A literature review of this field was provided in chapter 2, as well as numbers of preliminary work based on the experiments for mocrofluidic fuel cell modeling were discussed; The theoretical and numerical studies on microfluidic fuel cells were presented in chapter 3 and 4 respectively. In this chapter, conclusions and contributions will be presented, as well as the future work.

5.1 Conclusion and Contribution

A theoretical study about microfluidic fuel cells has been presented on three general aspects: such as mass transfer, hydrodynamics, and electrochemistry. Subsequently, we conducted a numerical analysis to study the performance of a laminar flow-based microfluidic fuel cell consisting of a Y-shaped microchannel. Three dimensional models for the microfluidic fuel cell have been developed in this work. The

models were applied to investigate species transport, hydrodynamics and electrochemical reaction in six domains of electrodes, catalyst layers, and microchannels. In this thesis the catalyst layers were modeled as two finite domains rather than just two boundaries. A laminar flow field is used to investigate the species transfer. Two conductive media DC modules representing electronic transport in the external circle and ionic transport in the internal circle respectively were used to model the electric fields within the fuel cell. The commercial software, COMSOL Multiphysics ®, was used to solve the governing equations numerically. A detailed analysis on the species transport and electrochemical reaction was put forward for an isothermal, single phase case. Afterward, a discussion about the effects of the convergence angle of the Y-shaped channel, the volumetric flow rate (pressure drop), the concentration of reactants, and the catalyst layers' porosities on the cell performances are given successively.

This numerical work uses the same conditions as the experimental work of Choban et al.(*4*) where the authors used a planar channel design, but for the numerical work it apply the straight channel and Y-shaped channel. The results show a good concordance and that the straight channel design numerical model provides 67% higher power density than the planar channel design experimental work. One the other hand, for the Y-shaped design, its performance is lower than the experimental work. However, the planar channel design requires a significant difference in density between the top flow and the bottom flow. This is not the case for the Y-shaped design. Most importantly, the power density of the ideal straight design is twice higher than Y-shaped design's, it indicates that there is significant potential space to improve the cell performance by modifying the channel geometry.

The first group of modeling on different convergence angles has confirmed that Y-shaped microchannel with 45° convergence angle has the maximum cell performance compared with 30°and 60° designs. The geometry of the cell plays a critical

role in the performance of the cell, which is limited by the mass transport of reactants through the concentration boundary layers to the electrodes.

After the Y-shaped microchannel with 45°convergence angle designed has been proved that provides a better cell performance, this design has been used to investigate cell models with three sets of pressure drops in the channel. The results show that the flow rate in the channel significantly effects the cell performance, because comparing 100 *Pa* and 60 *Pa* pressure drop, the cell performance was tremendously improved by 5 *Pa*. Therefore, lowering the inlet velocity from a high value results in a significant improvement in fuel utilization by increasing the reaction time of electrochemical reactions on the electrode surface with a minimal increase in cross stream mixing at the outlet; However, on the other hand, when the velocity goes too low, it will decrease the fuel utilization by consuming the reactant on the fuel crossover resulted from low flow rate.

After setting the convergence angle and pressure drop,the effects of concentration on cell performance has been examined . Firstly, it only considered the concentration of formic acid in the anode stream. It was expected that its influence should be small since the cell performance is primarily cathode-limited. Contrarily, the variation of oxygen concentration can particularly effect the cell performance, and elevating the concentration of oxygen in the solution can significantly improve the cell performance.

For the catalyst layers, a modeling study has been made on the porosity of them. Since the fuel cell is cathode-limited, the porosity of the anode catalyst layer plays a minor role only on the cell performance. The modeling of the cathode catalyst layer with different porosity showed that the 0.4 porosity case has the highest cell performance over the 0.5, 0.6, and 0.7 cases. Therefore, by modifying the catalyst layers can help improve the cell performance.

5.2 Future Directions

The present results provide an overview for the characteristics of this microfluidic fuel cell model and also benefit the further design work to optimize the cell performance. Some of opportunity for future work is outlined below.

From what it shows in Figure **??**, it still has a big difference on cell performance between this Y-shaped design modeling work and the theoretical ideal modeling design. It indicates that by improving the channel design in a better way, it still can significantly obtain a better cell performance.

Considering the oxygen concentration is an important factor effecting the cell performance and it is difficult to dissolve the gaseous oxygen into solution to obtain a high concentration, exploration of a new liquid oxidant is very interesting for future improvements.

Additionally, the microchannels have to continue to be tested and their length, width, and thickness optimized to give the maximum power density using a minimum physical area. As well as the material choosing for the channel fabrication can be done by Spark assisted chemical engraving (SACE) machining in Dr. Wuthrich's lab. SACE is a novel method for 3D microstructuring of glass or other nonconductive materials with high aspect ratio and smooth surface quality (*5*).

The catalyst layer has been always considered as one of the most significant aspects of cell performance improvement. Choosing different catalyst materials, and modifying the layer configuration could be investigated to enhance the electrochemical reaction, as well as the electrode design.

Finally, since the experimental work of Choban et al.(*4*) offers a better cell performance than the Y-shaped modeling work by using planar channel design, it will be very interesting to test our Y-shaped channel but with vertical planner design for

the specific case when there is a significant difference in density between the top flow and the bottom flow.

REFERENCES

[1] Bruus, H. Theoretical Microfluidics **2007**, 48 – 51.

[2] Leo J. M. J. Blomen, M. N. M. Fuel Cell Systems **1993**, 81 – 84.

[3] Chang, M.-H.; Chen, F.; Fang, N.-S. Analysis of membraneless fuel cell using laminar flow in a Y-shaped microchannel. *Journal of Power Sources* **2006**, *159*, 810 – 816.

[4] Choban, E. R.; Markoski, L. J.; Wieckowski, A.; Kenis, P. J. A. Microfluidic fuel cell based on laminar flow. *Journal of Power Sources* **2004**, *128*, 54 – 60.

[5] Wuthrich, R.; Fascio, V. Machining of non-conducting materials using electrochemical discharge phenomenon–an overview. *International Journal of Machine Tools and Manufacture* **2005**, *45*, 1095 – 1108.

[6] Kjeanga, E.; Djilali, N.; Sintona, D. Microfluidic fuel cells: A review. *Journal of Power Sources* **2009**, *186*, 353 – 2369.

[7] Bazylak, A.; Sinton, D.; Djilali, N. Improved fuel utilization in microfluidic fuel cells: A computational study. *Journal of Power Sources* **2005**, *143*, 57 – 66.

[8] Choban, E.; Markoski, L.; Stoltzfus, J.; Moore, J.; Kenis, P. Microfluidic Fuel Cells that Lack a PEM. *Power Sources Proc.* **2002**, *40*, 317 – 320.

[9] Martinelli, M.; Viktorov, V. Modelling of laminar flow in the inlet section of rectangular microchannels. *Journal of Micromechanics and Microengineering* **2009**, *19*, 025013 (9pp).

[10] Lee,; Jinkee,; Palmore,; R., G. T.; Tripathi,; Anubhav, Optimization of Microfluidic Fuel Cells Using Transport Principles. *Analytical Chemistry* **2007**, *79*, 7301 – 7307.

[11] Compton, R. G.; Pilkington, M. B. G.; Stearn, G. M. Mass Transport in Channel Electrodes. *Chemical Society* **1988**, *84*, 2155 – 2171.

[12] Ismagilov, R. F.; Stroock, A. D.; Kenis, P. J. A.; Whitesides, G.; Stone, H. A. Experimental and theoretical scaling laws for transverse diffusive broadening in two-phase laminar flows in microchannels. *Applied Physics Letters* **2000**, *76*, 2376–2378.

[13] Phirani, J.; Basu, S. Analyses of fuel utilization in microfluidic fuel cell. *Journal of Power Sources* **2008**, *175*, 261 – 265.

[14] Chen, W.; Chen, F. Theoretical approaches to studying the single and simultaneous reactions in laminar flow-based membraneless fuel cells. *Journal of Power Sources* **2006**, *162*, 1137 – 1146, Special issue including selected papers from the International Power Sources Symposium 2005 together with regular papers.

[15] Kjeang, E.; Michel, R.; Harrington, D. A.; Sinton, D.; Djilali, N. An alkaline microfluidic fuel cell based on formate and hypochlorite bleach. *Electrochimica Acta* **2008**, *54*, 698 – 705.

[16] Kjeang, E.; Michel, R.; Harrington, D. A.; Sinton, D.; Djilali, N. A Microfluidic Fuel Cell with Flow-Through Porous Electrodes. *Journal of the American Chemical Society* **2008**, *130*, 4000 – 4006.

[17] Kjeang, E.; McKechnie, J.; Sinton, D.; Djilali, N. Planar and three-dimensional microfluidic fuel cell architectures based on graphite rod electrodes. *Journal of Power Sources* **2007**, *168*, 379 – 390.

[18] Kjeang, E.; Proctor, B. T.; Brolo, A. G.; Harrington, D. A.; Djilali, N.; Sinton, D. High-performance microfluidic vanadium redox fuel cell. *Electrochimica Acta* **2007**, *52*, 4942 – 4946.

[19] Choban, E.; Spendelow, J.; Gancs, L.; Wieckowski, A.; Kenis, P. Membraneless laminar flow-based micro fuel cells operating in alkaline, acidic, and acidic/alkaline media. *Electrochimica Acta* **2005**, *50*, 5390 – 5398.

[20] Chen, F.; Chang, M.-H.; Hsu, C.-W. Analysis of membraneless microfuel cell using decomposition of hydrogen peroxide in a Y-shaped microchannel. *Electrochimica Acta* **2007**, *52*, 7270 – 7277.

[21] Lu, Y.; Reddy, R. G. Investigation of micro-PEM fuel cell using experimental and modeling methods. *Electrochimica Acta* **2009**, *54*, 3952 – 3959.

[22] Mann, R.; Amphlett, J.; Peppley, B.; Thurgood, C. Application of Butler-Volmer equations in the modelling of activation polarization for PEM fuel cells. *Journal of Power Sources* **2006**, *161*, 775 – 781.

[23] Cheddie, D. F.; Munroe, N. D. Three dimensional modeling of high temperature PEM fuel cells. *Journal of Power Sources* **2006**, *160*, 215 – 223.

[24] Al-Baghdadi, M. A. S.; Al-Janabi, H. A. S. Modeling optimizes PEM fuel cell performance using three-dimensional multi-phase computational fluid dynamics model. *Energy Conversion and Management* **2007**, *48*, 3102 – 3119.

[25] Yoon, S. K.; Fichtl, G. W.; Kenis, P. J. A. Active control of the depletion boundary layers in microfluidic electrochemical reactors. *Lab on a Chip* **2006**, *6*, 1516–1524.

[26] Spiegel, C. Modeling Micro Fuel Cells **2008**, 299 – 334.

[27] Zhao, T. Micro Fuel Cells **2009**, 105 – 106.

[28] Britz, D. Digital Simulation in Electrochemistry **2005**, 5.

[29] Cottrell, F. G. Residual current in galvanic polarization. *The Journal of Physical Chemistry* **1903**, *42*, 385 – 431.

[30] Chen, F.; Chang, M.-H.; Lin, M.-K. Analysis of membraneless formic acid microfuel cell using a planar microchannel. *Electrochimica Acta* **2007**, *52*, 2506 – 2514.

[31] Yazdani, A.; Shojai, L. Solution of a Scalar Convection-Diffusion Equation Using FEMLAB. *COMSOL Multiphysics User's Conference 2005 Boston* **2005**.